nature chemical biology

Article

https://doi.org/10.1038/s41589-023-01353-y

Polarized focal adhesion kinase activity within a focal adhesion during cell migration

Received: 26 October 2022

Accepted: 3 May 2023

Published online: 22 June 2023

Check for updates

Xiaoquan Li[1,2], Joseph Dale Combs III[3], Khalid Salaita[3] & Xiaokun Shu[1,2]

Focal adhesion kinase (FAK) relays integrin signaling from outside to inside cells and contributes to cell adhesion and motility. However, the spatiotemporal dynamics of FAK activity in single FAs is unclear due to the lack of a robust FAK reporter, which limits our understanding of these essential biological processes. Here we have engineered a genetically encoded FAK activity sensor, dubbed FAK–separation of phases-based activity reporter of kinase (SPARK), which visualizes endogenous FAK activity in living cells and vertebrates. Our work reveals temporal dynamics of FAK activity during FA turnover. Most importantly, our study unveils polarized FAK activity at the distal tip of newly formed single FAs in the leading edge of a migrating cell. By combining FAK–SPARK with DNA tension probes, we show that tensions applied to FAs precede FAK activation and that FAK activity is proportional to the strength of tension. These results suggest tension-induced polarized FAK activity in single FAs, advancing the mechanistic understanding of cell migration.

Signal transduction from the environment to inside cells has essential roles in modulating cell adhesion and motility[1]. Within this signaling pathway, focal adhesion kinase (FAK) is a critical component in sensing and integrating extracellular cues to control cell motility[2,3]. FAK activity regulates dynamic formation of cell adhesions and membrane protrusions, which controls cell movement[2]. In particular, FAK influences focal adhesion (FA) turnover, including FA assembly and disassembly[4]. FA is a critical structure in connecting extracellular matrix to intracellular structures, including actin filament[5]. During cell movement, including spreading and migration, integrin–matrix interaction triggers FA formation, which anchors cells to the substrate and provides traction force for actin polymerization-induced membrane protrusion. Therefore, spatiotemporal control of FAK activity is essential in regulating FA dynamics. To further understand the role of FAK during cell spreading and migration, it is ideal to visualize real-time FAK activation in single FAs with spatial and temporal resolution.

To achieve spatiotemporal resolution, it is preferred to use a genetically encoded fluorescent reporter in imaging FAK activity. Such a reporter should have large dynamic range, that is large fluorescence change upon FAK activation, which will enable robust reporting of FAK activation. It should also provide high spatial resolution in single FAs so that FAK activity can be reported during FA turnover. And it should have a good temporal resolution that is within the temporal range of FA dynamics. Although Förster resonance energy transfer (FRET)-based FAK activity reporters using autofluorescent green fluorescent protein (GFP) and its variants have been developed[6], these FRET-based reporters suffer from weak signal, with small fluorescence changes upon FAK activation, and they lack spatial resolution in imaging FAK activity in single FAs. Here we designed a versatile and robust FAK activity reporter by using a new principle-based approach—GFP phase separation via multivalent interactions that are induced by FAK activity-dependent phosphorylation. We named this FAK reporter FAK–separation of phases-based activity reporter of kinase (SPARK). FAK–SPARK forms intensely bright droplets upon FAK activation in living cells and vertebrate animals. FAK–SPARK achieves excellent spatiotemporal resolution and visualizes endogenous FAK activity within single FAs during their assembly and disassembly.

Results

Designing a FAK reporter by GFP phase separation

To develop FAK–SPARK so that we can induce GFP phase separation by active FAK, we designed a multivalent interaction system. First, we

[1]Department of Pharmaceutical Chemistry, University of California San Francisco, San Francisco, CA, USA. [2]Cardiovascular Research Institute, University of California San Francisco, San Francisco, CA, USA. [3]Department of Chemistry, Emory University, Atlanta, GA, USA. e-mail: xiaokun.shu@ucsf.edu

fused a FAK-derived substrate peptide containing tyrosine 397 (Y397) to enhanced GFP (EGFP). This substrate peptide has been widely used in the FRET-based biosensors[6] and is well known to be specifically phosphorylated by FAK (and thus we named it FAKsub). Second, we fused the phosphopeptide-binding domain SH2 to a nonfluorescent variant of GFP (denoted as EGFP* that contains Y66F mutation). Third, we fused a multivalent tag named homo-oligomeric tag (HOTag) to each of the above constructs, which introduces multivalency (Fig. 1a)[7,8]. Here the hexameric tag homo-oligomeric tag 3 (HOTag3) is fused to FAKsub–EGFP. And a tetrameric tag homo-oligomeric tag 6 (HOTag6) is fused to SH2–EGFP*. The two HOTags are de novo-designed coiled coils[8]. Finally, to express the two parts in one construct, we linked the two parts with the 'self-cleaving' 2A sequence (Supplementary Table 1). Thus, when FAK is activated, the FAKsub is phosphorylated, resulting in its interaction with SH2 (Fig. 1b). Together with the multivalent HOTags, this drives phase separation of EGFP through multivalent interaction. Specifically, each hexameric FAKsub–EGFP–HOTag3 recruits six SH2–EGFP*–HOTag6, and each tetrameric SH2–EGFP*–HOTag6 recruits four FAKsub–EGFP–HOTag3. This multivalent interaction-driven crosslinking and phase separation lead to phase separation of EGFP, forming intensely bright droplets (Fig. 1b).

To demonstrate and characterize FAK–SPARK, the reporter was expressed in HEK293 cells, which showed punctate fluorescence in the cytoplasm (Fig. 1c). This is in contrast to the homogeneous fluorescence from a mutant reporter, in which the Y397 was mutated to phenylalanine (F) so that it cannot be phosphorylated by FAK. Because of multivalent interactions in the droplets, this would likely perturb EGFP fluorescence lifetime. Indeed, using fluorescence lifetime imaging microscopy (FLIM), we found that the EGFP fluorescence lifetime in the droplets is shorter than that in the diffuse state (that is homogenously distributed GFP; Supplementary Fig. 1; Methods). These data suggest that the multivalent interactions induced EGFP droplet formation and that FAK–SPARK reports FAK activity in the cells. To further confirm this, we incubated the cells with FAK inhibitor PF-562271, which inhibited punctate fluorescence. In comparison, incubation with dimethyl sulfoxide (DMSO) did not inhibit the punctate structure of FAK–SPARK. To analyze the imaging data in a quantitative way, we defined 'SPARK signal', which is the ratio of summarized fluorescent droplets' pixel intensity divided by summarized cells' pixel intensity (Fig. 1d). Thus, 'SPARK signal' measures the percentage of GFP in the droplet form over the total. SPARK signal-based analysis confirmed that the FAK inhibitor blocked droplet formation, and the droplet formation was dependent on Y397 phosphorylation (Fig. 1d). Next, we characterized that the reporter droplets were reversible upon the addition of the FAK inhibitor. Time-lapse imaging showed that half-to-maximum time ($T_{1/2}$) was ~30 min (Fig. 1e and Supplementary Fig.2). We further showed recovery of reporter droplets after washing out the inhibitor (Extended Data Fig. 1). Thus, FAK–SPARK is reversible in reporting FAK activity. We also confirmed that FAK–SPARK could detect FAK activity in various cancer cells (Extended Data Fig. 2).

Finally, we demonstrated that FAK–SPARK was able to detect FAK activity in living vertebrate animals. First, we created a transgenic zebrafish that is referred to as 'Tg(UAS–FAK–SPARK)' in which the FAK–SPARK reporter is under the UAS promoter. Next, we crossed it with the transgenic zebrafish TgBAC (ΔNp63:Gal4FF)la213 so that the reporter is expressed in the basal epithelial cells in which mCherry is also expressed by UAS–mCherry[9]. Imaging in the tail bud of zebrafish at 48 h postfertilization showed bright green fluorescent droplets, whereas mCherry showed homogenous red fluorescence (Fig. 1f). In contrast, the transgenic zebrafish expressing the Y397F variant reporter that does not respond to FAK showed homogeneous green fluorescence in the same region. These data indicate that FAK–SPARK reports FAK activity in the live and intact zebrafish. Therefore, FAK–SPARK will be a useful tool for imaging FAK activity in animals.

FAK activation follows the assembly of FAs during cell spreading

We first demonstrated that FAK–SPARK achieved spatiotemporal resolution in detecting FAK activity using the synthetic system by targeting the constitutively active FAK (CA–FAK, amino acid 355–690 of FAK) to specific locations in cells[10]. First, we targeted CA–FAK to the centrosome by fusing it to Aurora A kinase and a red fluorescent protein mKO3 (refs. 11,12). Co-expression of this CA–FAK fusion and FAK–SPARK revealed GFP droplets in the centrosome (Extended Data Fig. 3a)[13]. In contrast, no FAK–SPARK droplets were observed in the centrosome of cells without co-expression of the CA–FAK fusion protein. Second, we targeted CA–FAK to nuclear condensates by fusing it to nuclear homo-oligomeric tag 1 (HOTag1) condensates, tagged with mKO3. Previously, we showed that HOTag1 formed condensates[8]. For nuclear localization, we fused the nuclear localization signal (NLS) to HOTag1. Co-expression of the CA–FAK fusion and FAK–SPARK showed green droplets in the nucleus, which are colocalized with the red condensates, indicating that FAK–SPARK reports FAK activity in the expected locations (Extended Data Fig. 3b). Together, our data using CA–FAK demonstrate that FAK–SPARK enables imaging of FAK activity with spatial resolution in living cells. On the other hand, because the reporter droplets would no longer have interaction with the active FAK, in locations with intracellular fluid flow, the droplets may drift away from the active FAK, resulting in loss of spatial resolution. Thus, we suggest that, in general, the formation of FAK–SPARK droplets should be monitored to determine the location of active FAK (see Fig. 2b and related description).

Next, we characterized temporal resolution of FAK–SPARK using a small molecule-inducible tagging of CA–FAK to the nuclear HOTag1 condensates (Extended Data Fig. 3c). In particular, we fused Frb to the mKO3-labeled nuclear HOTag1 condensates (HOTag1–NLS–mKO3–Frb) and fused FKBP to a near-infrared fluorescent protein 2 (IFP2)-labeled CA–FAK that located in the cytosol (FKBP–IFP2–CA–FAK)[14–16]. Upon addition of rapamycin[17], CA–FAK translocated into the nucleus and localized to the HOTag1 condensates (Extended Data Fig. 3c). Time-lapse imaging showed that near-infrared fluorescent droplets appeared in the nuclear condensates at around 5 min after the addition of rapamycin (Extended Data Fig. 3d). FAK–SPARK formed droplets at around 6–7 min after addition of rapamycin. Furthermore, the near-infrared CA–FAK droplets were colocalized with the red HOTag1 condensates, suggesting that CA–FAK were indeed translocated to the HOTag1 condensates as expected via rapamycin-mediated FKBP and Frb interaction (Extended Data Fig. 3e). The green FAK–SPARK droplets were colocalized with near-infrared CA–FAK droplets, indicating that FAK–SPARK reports active CA–FAK with spatial resolution (Extended Data Fig. 3e). Quantitative analysis of the time-lapse imaging data showed that SPARK signal of near-infrared CA–FAK appeared first, ~1 min to 2 min earlier than the SPARK signal of the green FAK–SPARK, while SPARK signal of the HOTag1 droplets was relatively stable over time (Extended Data Fig. 3f and Supplementary Video 1). Thus, FAK–SPARK achieves a temporal resolution of 1–2 min in reporting FAK activation by the CA–FAK.

We next applied it to visualize the dynamics of FAK activity during cell spreading. We transfected FAK–SPARK into cells, with co-expression of a red fluorescent protein mApple-fused paxillin that labels FAs[18]. To induce and visualize cell spreading, we detached and reseeded cells 24 h after transfection. Approximately 1–2 h after reseeding, the cells re-attach and spread[19]. We then conducted time-lapse imaging of the cell-spreading process (Fig. 2a). First, cells increased area outward over time, indicating cell spreading (Fig. 2b). Meanwhile, small FAK–SPARK droplets were generated from the leading edge, and moved inward, likely driven by the retrograde flow. Zoom-in images showed that the small droplets were produced in the FAs and moved toward the center of cells (Fig. 2b, inset). Quantitative analysis of the imaging data showed that the area of the spreading cell increased over time and that FAK–SPARK signal also increased. Furthermore, the

https://doi.org/10.1038/s41589-023-01353-y

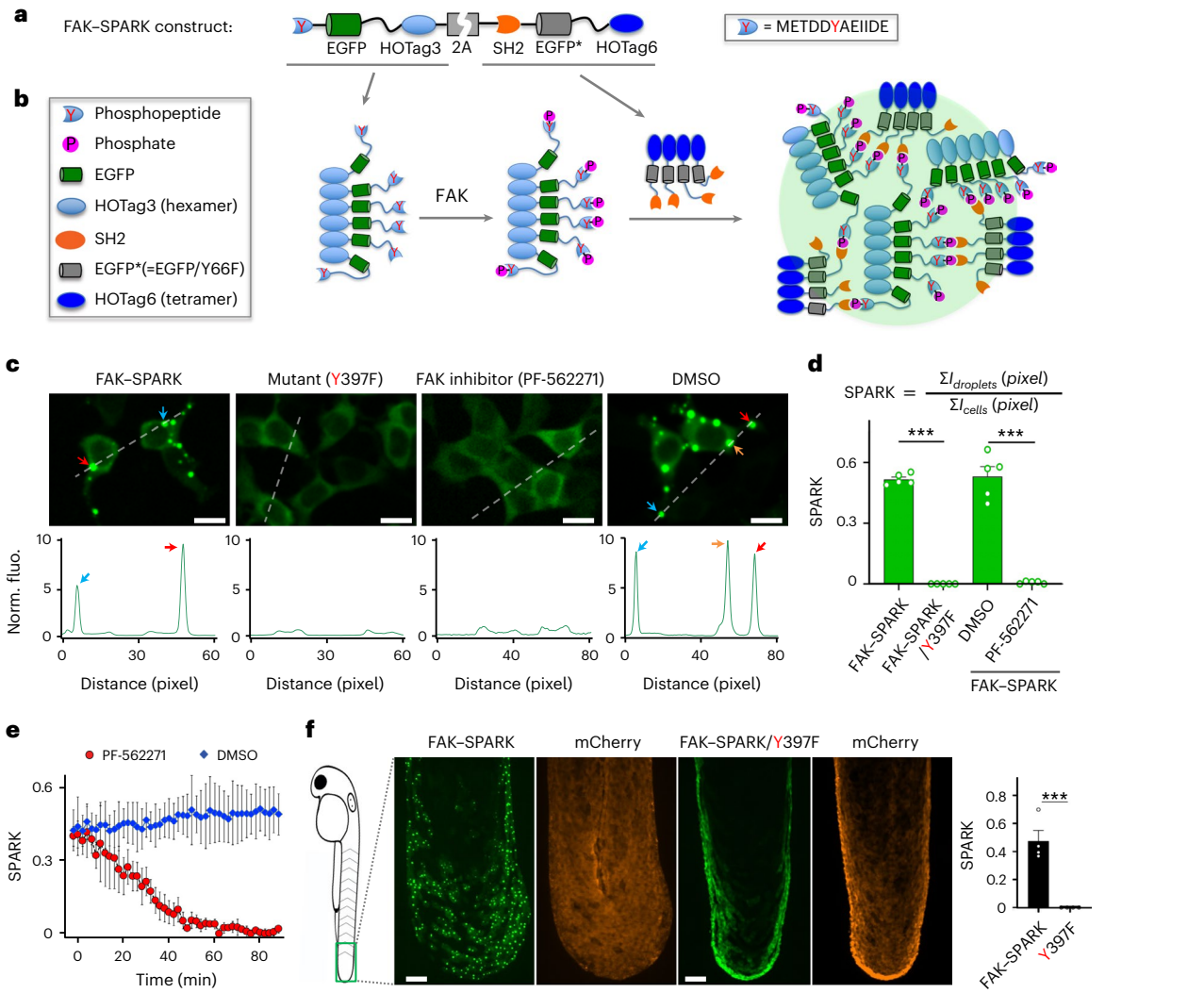

Fig. 1 | Phosphorylation-induced GFP phase separation-based FAK reporter visualizes the endogenous activity of FAK in living cells and vertebrates. **a**, Schematic representation of construct of FAK reporter FAK–SPARK. **b**, Working mechanism of FAK–SPARK. **c**, Top: two left panels, fluorescence images of cells expressing FAK–SPARK, FAK–SPARK mutant Y397F that cannot be phosphorylated by FAK; two right panels, fluorescence images of cells expressing FAK–SPARK incubated with FAK inhibitor or DMSO. Bottom: histogram along the dashed line. This experiment was repeated three times independently with similar results. **d**, Quantified SPARK signal in cells with various conditions, $n = 5$ biological replicates, two-sided nonpaired t-test. $P = 9.65 \times 10^{-11}$ between 'FAK–SPARK and FAK–SPARK/Y397F' and $P = 4.66 \times 10^{-6}$ between 'DMSO and PF-562271'. **e**, FAK–SPARK is reversible upon the addition of FAK inhibitor, $n = 3$ biological replicates. **f**, Left: schematic representation of zebrafish. Middle: fluorescence images of transgenic zebrafish expressing FAK–SPARK or FAK–SPARK/Y397F. Tg (UAS–FAK–SPARK or FAK–SPARK/Y397F) was crossed with Tg (ΔNp63:GAL4) and Tg (UAS–mCherry). Right: quantified SPARK signal, $n = 4$ biological replicates, two-sided nonpaired t-test. $P = 0.0008$. Data are mean ± s.e.m; ***$P < 0.001$. Scale bars, 20 μm (**c**,**f**).

increase of FAK–SPARK signal is well correlated with the increase of cellular area (Fig. 2b, right). This suggests that during the cell spreading, FAK is activated, which mainly occurred in the leading edge at early spreading (Supplementary Video 2).

FAK–SPARK droplets were not only produced in the leading edge (Supplementary Video 3) but also produced during the assembly of FAs in the area away from the leading edge (Supplementary Video 4). Time-lapse imaging revealed that following assembly of single FAs, which were visualized by mApple–paxillin, FAK–SPARK droplets formed within single FAs (Fig. 2c). Quantitative analysis of the FA growth and FAK–SPARK signal within this single FA region showed that FA growth precedes the FAK–SPARK signal (Fig. 2c, right), indicating that FAK activation follows FA assembly. Furthermore, the green droplets were generated in the single FA in a temporal order following the growth direction of the single FA (Fig. 2c, time series insets at 108 min and 118.5 min, and Supplementary Video 5).

FAK activity precedes FA disassembly

Because previous studies showed that FAK activity is required for the disassembly of FAs[4], we imaged FAs and FAK activity in living cells. Time-lapse imaging revealed that before the disassembly of FAs in a stationary cell, FAK–SPARK droplets appeared first in the single FAs (Fig. 3a and Supplementary Video 6). Quantitative analysis showed that FAK was inactive and became activated before FA disassembly (Fig. 3a, right, and Supplementary Video 7). Our data, thus, indicate that FAK activation precedes disassembly events of FAs, which is consistent with previous studies showing essential roles of FAK in FA disassembly[20,21].

FA 'sliding' has also been reported previously[22,23], and we observed such events in the spreading cells. FAK–SPARK droplets were produced in the sliding FAs (Fig. 3b and Supplementary Video 8). Quantitative analysis indicated that FAK was active during FA sliding events (Fig. 3b, right). At the late stage of cell spreading, the cellular area had little change, but FAK–SPARK droplets were still generated in the edge of cells

https://doi.org/10.1038/s41589-023-01353-y

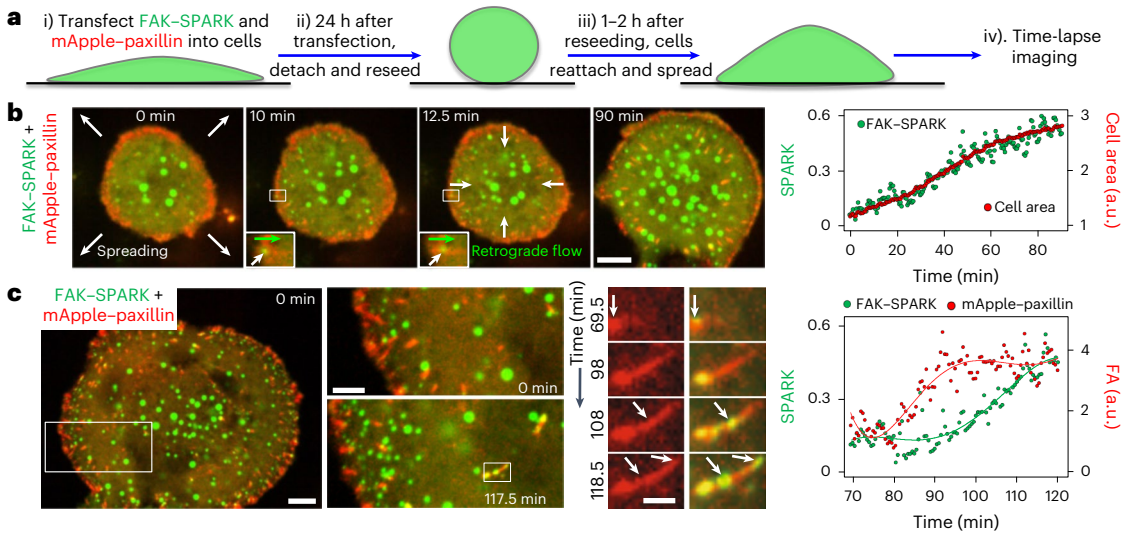

Fig. 2 | FAK–SPARK detects FAK activation during cell spreading and visualizes FAK activity within single FAs after FA assembly. a, Experimental procedure. **b**, Left: time-lapse images during cell spreading. Right: normalized SPARK signal (green) and cell area (red) over time. **c**, Left: time-lapse images during FA assembly and FAK activation within FAs (middle). Right: normalized SPARK signal and FA over time. Three independent repetitions of **b** and **c** had similar results. Scale bars, 10 µm (**b**); 10 µm (left), 5 µm (middle) and 2 µm (right) (**c**).

(Supplementary Video 9). Time-lapse imaging in the periphery of cells showed that FAs assembled (Fig. 3c, yellow arrows) and disassembled (Fig. 3c, blue arrows) over time and that FAK–SPARK droplets were generated in the FAs undergoing turnover (Fig. 3c and Supplementary Video 10). Therefore, our imaging data showed that FAK–SPARK visualized FAK activity during FA dynamic turnover in cells.

We also examined whether the expression of the additional substrate from FAK–SPARK would perturb FA dynamics and cell behavior. Here we characterized the dynamics of FAs, including the FA assembly and disassembly rate in FAK–SPARK sensor-expressing cells, and compared them to the control cells expressing GFP. We found that the FA assembly and disassembly rates are similar with no significant difference between the FAK–SPARK-expressing cells and the control (Extended Data Fig. 4). This suggest that FAK–SPARK expression does not perturb FA assembly and disassembly. To examine if FAK–SPARK expression perturbs cell behavior, we characterized cell migration rate using a wound-healing assay and found that cells expressing the reporter showed a similar migration rate in comparison to the control cells (Extended Data Fig. 5). Taken together, our data, thus, suggest that expression of the reporter does not perturb FA dynamics and cell behavior such as migration.

Polarized FAK activity in newly formed FA at the leading edge

After late spreading, cells start to migrate[19]. We imaged FAK activity at the leading edge of the migrating cells (Fig. 4a). Briefly, we transfected FAK–SPARK and mApple–paxillin into HeLa cells, which were then reseeded and allowed to re-attach and spread. FAK–SPARK visualized green droplets, which were produced in the distal tip of newly formed FAs in the leading edge (Fig. 4b–d). Quantitative analysis of the fluorescence intensity confirmed that FAK–SPARK droplets were distributed in the distal tip of single FAs (Fig. 4d, right). These droplets then dissociated from the FAs and moved toward the cell body due to retrograde flow (Supplementary Video 11). This is likely because, after FAK-induced phosphorylation of the reporter's substrate peptide, the phosphorylated substrates will no longer interact with FAK. Thus, after phosphorylation, the FAK–SPARK droplets will no longer interact with FAK, and with the retrograde flow in the leading edge, they moved toward the cell body. This is also partly due to the relatively long lifetime of the droplets, which is ~20 min (Supplementary Fig. 3). These FAK–SPARK droplets' flow speed is ~0.5 µm min^{-1} to 1.5 µm min^{-1}, which is consistent with the reported actin retrograde flow ~0.6 µm min^{-1} to 1.8 µm min^{-1} (ref. 24). Furthermore, these droplets became larger on their way toward the cell center because the smaller droplets fuse together during their movement.

We also verified that FAK was distributed along the entire FA using a near-infrared IFP2-tagged FAK (Fig. 4e,f)[13,15,25]. We further used immunostaining against the endogenous FAK, which indicated that the endogenous FAK was distributed along the entire FA (Supplementary Fig. 4). In contrast, newly formed FAK–SPARK droplets were found in the distal tip of the newly formed FAs in the leading edge of a migrating cell. Statistical analysis of over 40 single FAs showed that the formation of FAK–SPARK droplets occurred in the distal tip of these newly formed FAs in the leading edge of migrating cells (Fig. 4g). Furthermore, immunostaining with an antibody against FAK pY397 showed that FAK–SPARK droplet signal colocalized with peak signal of FAK pY397, demonstrating that the sensor reports polarized FAK pY397 signal (Supplementary Fig. 5). Thus, our data suggest that although FAK is distributed in both the distal and proximal tip of FAs, the active FAK is mainly found in the distal tip of FAs in the leading edge.

Based on our results and current understanding of FAK activation mechanisms, we propose a model (Fig. 4h) to interpret the polarized FAK activity in single FAs at the leading edge (Discussion). Briefly, membrane protrusion is induced by actin polymerization in the leading edge of a migrating cell. Actin contraction generates forces, which are likely stronger when closer to the membrane. Through the FAs and integrin–extracellular matrix (for example, fibronectin (FN)) interaction, the actin contractibility-generated force is transmitted to FAK, which, on the one hand, is connected to actin filament via actin–vinculin–paxillin–FAK[26] by binding to paxillin via its focal adhesion targeting (FAT) domain, or via actin–Arp2/3–FAK[27,28], and on the other hand, is anchored to the cell membrane via interaction of FERM (F for 4.1 protein, E for ezrin, R for radixin and M for moesin) with phosphatidylinositol 4,5-bisphosphate (PI(4,5)P2)[29,30]. The tension on FAK dissociates the inhibitory FERM domain from the kinase domain, initiating FAK activation. Our model suggests that the closer an FA is to the membrane protrusion, the stronger the actin contractibility-induced force and the stronger the tension on the FA (and FAK), resulting in polarized FAK activity along single FAs at the leading edge of a migrating cell.

https://doi.org/10.1038/s41589-023-01353-y

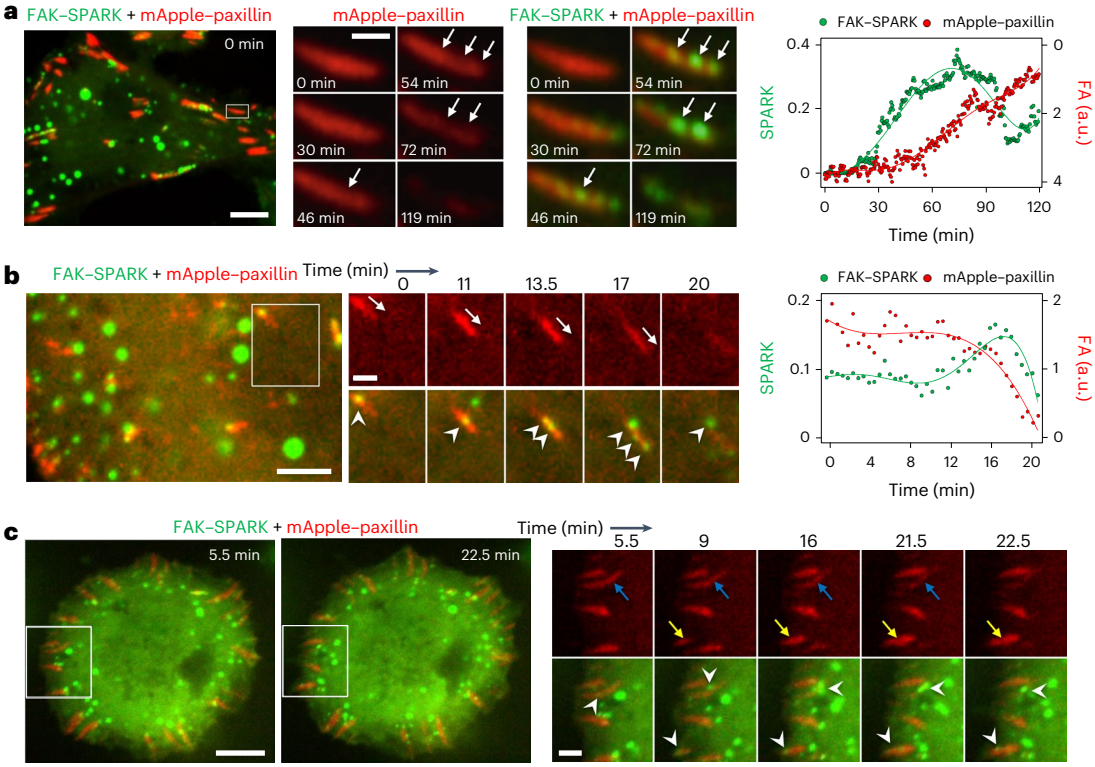

Fig. 3 | FAK is activated before the disassembly of FAs or during sliding and turnover. a, Left: fluorescence images showing FAK activation within single FAs before disassembly in a stationary cell. Right: normalized SPARK signal and FAs over time. **b**, Left: fluorescence images showing FAK activation within single FAs during sliding. Right: normalized SPARK signal and FAs over time. **c**, Fluorescence images showing FAK activation during assembly and disassembly of FAs in a late spreading cell. Three independent repetitions of **a**–**c** had similar results. Scale bars, 10 μm (left) and 2 μm (right) (**a**); 5 μm (left) and 2 μm (right) (**b**); 10 μm (left) and 3 μm (right) (**c**).

Polarized FAK activity depends on inhibitory FERM domain

According to the above model, the inhibitory FERM domain is one critical component for the polarized activity of FAK in single FAs at the leading edge. To test this, we decided to target CA–FAK to the FAs at the leading edge and examine whether FAK–SPARK droplets would be generated without polarization. We knocked down endogenous FAK by short hairpin RNA (shRNA) against the c-terminal region of FAK (between 854 and 860 amino acids; Supplementary Fig. 6). Knockdown of FAK abolished FAK–SPARK droplets in cells (Supplementary Fig. 6). We then fused CA–FAK to mApple–paxillin and expressed the fusion protein, which rescued FAK activity in cells (Supplementary Fig. 6). Time-lapse confocal microscopic imaging of single FAs revealed that FAK–SPARK droplets were generated at proximal, center, and distal tip of FAs at the leading edge of migrating cells that expressed FA-targeted CA–FAK (Fig. 5a and Supplementary Video 12). Statistical analysis of ~40 single FAs showed that FAK activity is no longer polarized at the distal tip (Fig. 5b). Furthermore, we confirmed that re-expression of the wild-type full-length FAK (wtFAK) in these cells showed polarized activity of FAK (Supplementary Fig. 7). Interestingly, CA–FAK enhanced FA assembly and disassembly rate compared to the wild-type full-length FAK (Supplementary Fig. 8). Taken together, our results indicate that the FERM domain is critical for the polarized FAK activity, which is consistent with the proposed model (Fig. 4h).

FAK activity depends on integrin and actin contractibility

To further support the proposed model, we next examined whether the detected FAK activity is dependent on integrins that bind FN. $\alpha5\beta1$ is one of the main integrins in HeLa cells that also express αvβ5 and αvβ3 (ref. 31). Incubation of cells with $\alpha5\beta1$ inhibitors reduced FAK activity in a dose-dependent manner (Fig. 5c,d)[32]. Antibody against $\alpha5\beta1$ also blocked FAK activity[32]. These data demonstrate that FAK activity does depend on integrins, which is consistent with the proposed model.

Next, we perturbed the actin cytoskeleton and examined whether this affects FAK activity. Incubation with blebbistatin, a myosin II inhibitor[33], reduced FAK activity (Fig. 5e). Actin polymerization inhibitor, cytochalasin D[30], also blocked FAK activity. Furthermore, Rho-kinase inhibitor, Y27632 (ref. 34), also inhibited FAK activity. We also confirmed the observed reduction of FAK activity by determining FAK pY397 levels using western blot analysis, which showed that pY397 level was largely reduced upon treatment with the drugs (Supplementary Fig. 9). These data indicate that actin contraction contributes to FAK activation, which is consistent with the previous studies[18,30] and the proposed model (Fig. 4h).

Finally, we examined several FAK variants that were previously reported to have altered activity or interaction with the plasma membrane. We blocked basal FAK activity by co-expressing a dominant-negative FAK that is comprised of the FRNK domain[35,36]. Then we expressed various FAK variants and FAK–SPARK. First, expression of the wild-type (WT) FAK rescued FAK activity as expected. Second, expression of FAK variant Y180A/M183A, which has reduced affinity between FERM and the kinase domain[29], showed higher FAK activity than WT FAK, which is consistent with the consensus that the FERM domain interacts and inhibits the kinase (Fig. 4f). Third, the KAKTLRK motif at the FERM domain has been characterized to be responsible for binding to PI(4,5)P2 via the positively charged lysine and arginine because mutation of these basic residues to alanine blocked FAK interaction with PI(4,5)P2 (ref. 29). Expression of this FAK variant showed little FAK activity, which is consistent with our model (Fig. 4h). Finally, expression of the kinase domain from 355 to 690 amino acids (that is CA–FAK) showed the strongest FAK activity among the variants

https://doi.org/10.1038/s41589-023-01353-y

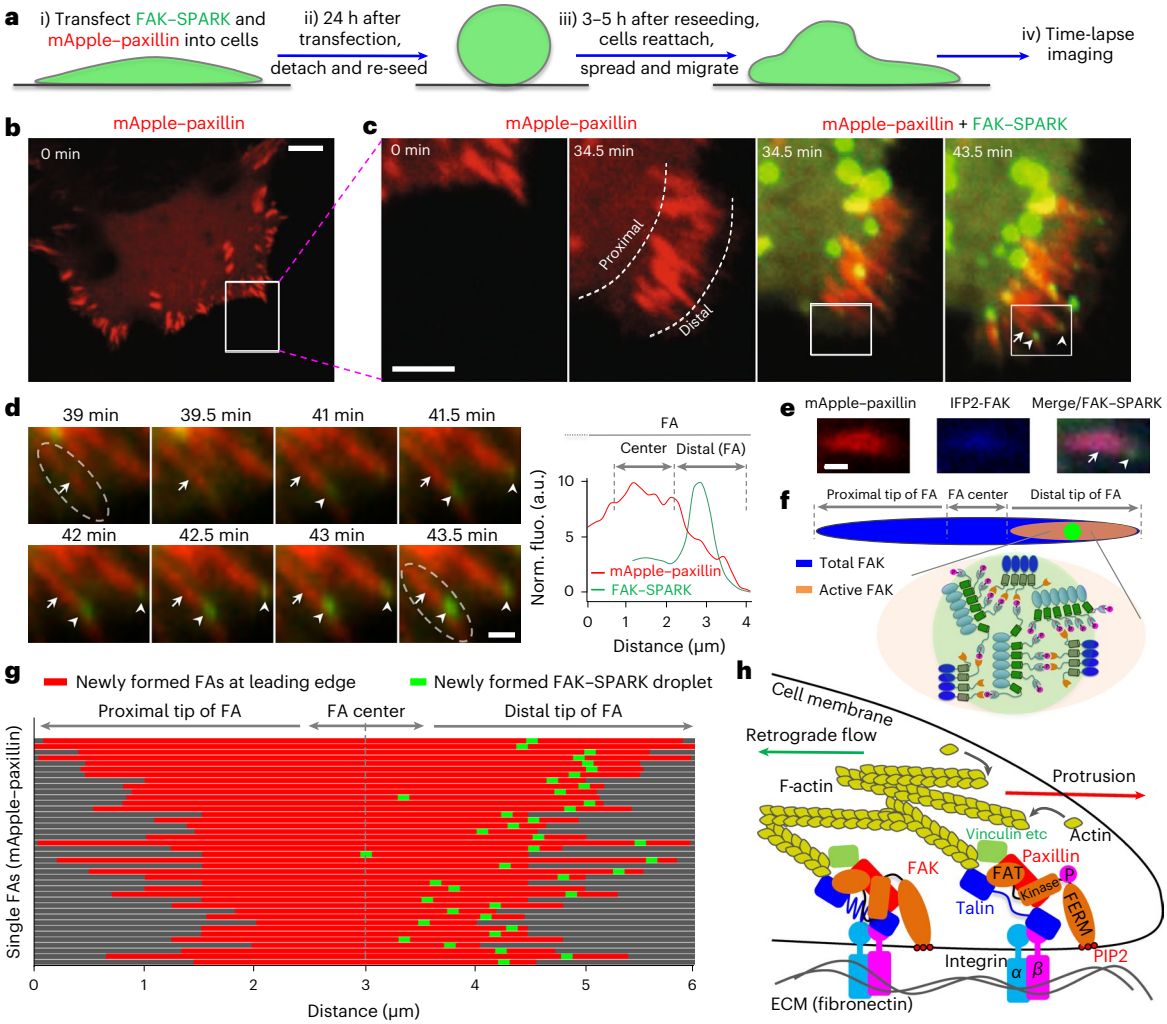

Fig. 4 | FAK activity is polarized at the distal tip of newly formed FAs in the leading edge. a, Experimental procedure. **b**,**c**, Time-lapse images of cells expressing mApple–paxillin and FAK–SPARK. **d**, Left: fluorescence images of the boxed area in **c**. Right: normalized fluorescence intensity over distance along the single FA (dashed box at 43.5 min). **e**, Fluorescence images. **f**, Distribution of total FAK and activated FAK within single FAs. **g**, Distribution of newly formed FAK–SPARK droplets in single FAs at the leading edge. **h**, Proposed model showing polarized FAK activation in single FAs at the leading edge of a migrating cell. Three independent repetitions of **b**–**e** had similar results. Scale bars, 10 μm (**b**), 5 μm (**c**), 1 μm (**d**) and 2 μm (**e**).

(Fig. 5f). Addition of the FERM domain to this CA–FAK, that is, 1–690 amino acids, substantially reduced FAK activity to a level similar to that of WT FAK (Fig. 5f).

Integrin–ECM ligand tension drives FAK activation

We first showed that integrin–ECM ligand tension precedes FAK activity. To investigate the relationship between integrin–ECM mechanical tension events and FAK activity, we needed to simultaneously image integrin tension while also imaging FAK–SPARK activity. We used molecular tension fluorescence microscopy (MTFM), which was developed in our group and has been broadly used to study mechanotransduction[37–40]. MTFM enables the mapping of piconewton (pN) tension events between individual integrin and their ligands. We used DNA-based MTFM probes that are highly tunable and are the most sensitive class of force sensors[39]. These probes are comprised of a folded DNA hairpin structure that is tagged with a Cy3B fluorophore and BHQ2 dark quencher pair positioned at the base of the stem region (Extended Data Fig. 6a)[41]. The probe is assembled from the following three strands: a ligand strand that carries the fluorophore, an anchoring strand that presents the quencher and a hairpin strand with arms complementary to the ligand and anchor strands (Extended Data Fig. 6a and Supplementary Figs. 10–13). When the hairpin is in a closed state, the fluorophore is quenched. Upon hairpin opening, induced by integrin–ligand tension, the fluorophore is dequenched and becomes 10–20 times brighter[39]. MTFM has a spatial resolution of conventional fluorescence microscopy and can be conveniently imaged in tandem with the FAK–SPARK signal[37]. We focused on investigating the initial 20–60 min period of cell-substrate spreading because this involves the formation of nascent FAs in which paxillin is recruited and integrin–substrate traction force begins to mount[39].

DNA hairpin tension probes are threshold reporters and generate signal when the applied force exceeds the $F_{1/2}$, which is defined as the equilibrium force that leads to a 50% probability of unfolding[41]. We designed tension probes with $F_{1/2}$ = 19 pN (Supplementary Fig. 12 and Supplementary Table 2), given that this magnitude of tension is associated with integrin activation and FA maturation[42]. Probes presented the cyclic Arg-Gly-Asp-d-Phe-Lys (cRGD) FN mimetic peptide that primarily engages $\alpha_v\beta_3$ and $\alpha_5\beta_1$ integrins (Extended Data Fig. 6a and Supplementary Fig. 10)[43]. When IFP2–paxillin and FAK–SPARK transfected HeLa cells were plated on MTFM-functionalized surfaces, cells rapidly spread on the surface as observed from reflection interference contrast microscopy (RICM). Fluorescence imaging at 20 min after plating cells

https://doi.org/10.1038/s41589-023-01353-y

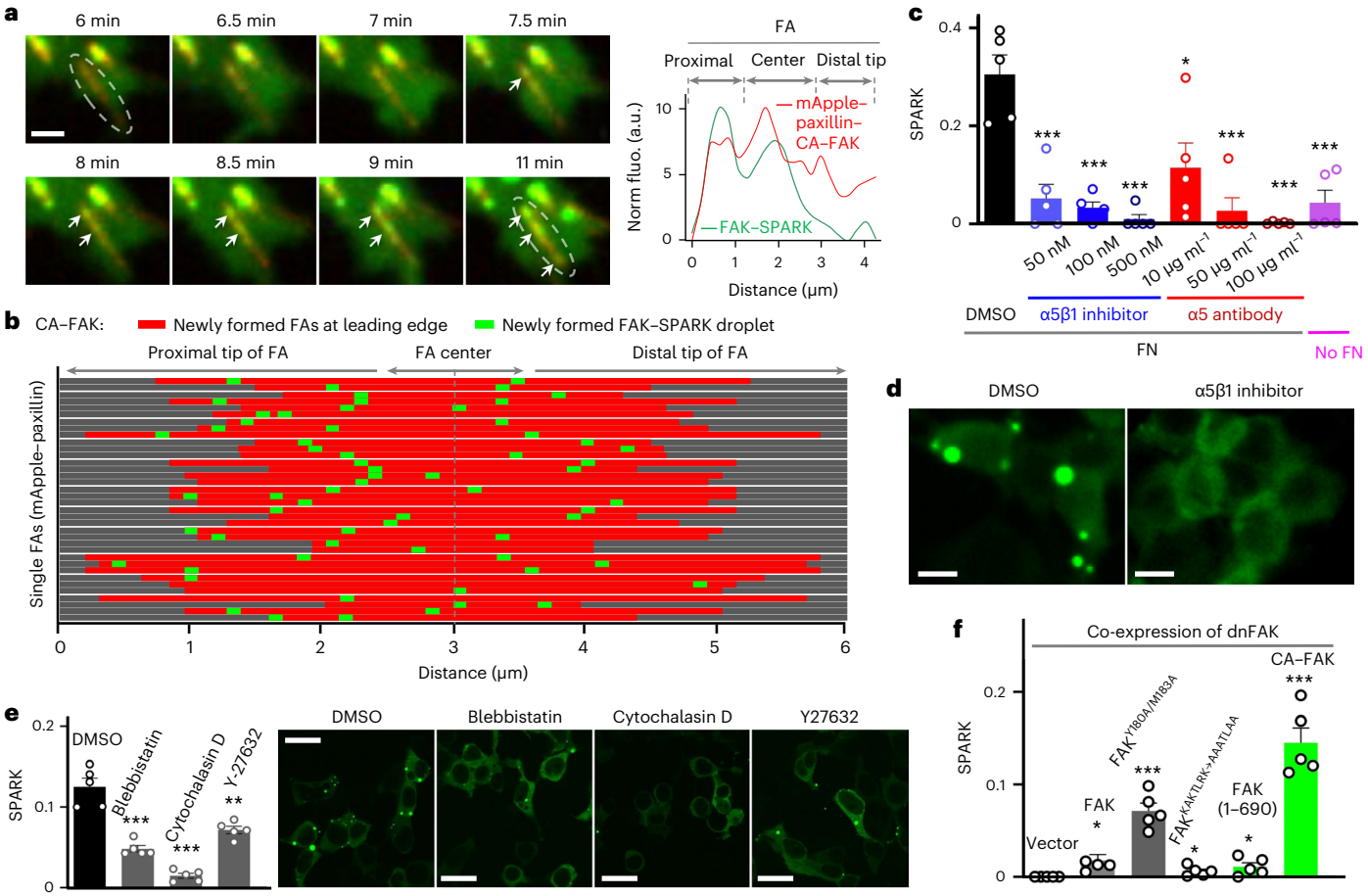

Fig. 5 | Polarization of FAK activity depends on FERM domain, integrin and actin cytoskeleton. a, Left: fluorescence images showing no distal polarization of FAK activity when CA–FAK is fused to paxillin and targeted to FAs in cells with endogenous FAK knocked down by shRNA against FAK (details in text). Right: normalized fluorescence over distance along the single FA (boxed area at 11 min). This experiment was repeated three times independently with similar results. **b**, Distribution of newly formed FAK–SPARK droplets in single FAs at the leading edge. **c**, Normalized SPARK signal in cells incubated with integrin inhibitors or antibodies. Cells were grown on fibronectin, $n = 5$ biological replicates, two-sided nonpaired t-test between DMSO and other treatments, exact P values are (from left to right bars) = 0.00086, 0.00018, 9.01×10^{-5}, 0.018, 0.00040, 6.18×10^{-5} and 0.00055. **d**, Representative images of cells expressing FAK–SPARK, incubated with DMSO or integrin inhibitor. This experiment was repeated five times independently with similar results. **e**, Left: normalized SPARK in cells incubated with inhibitors of myosin II, actin polymerization and ROCK. Right: representative images, $n = 5$ biological replicates, two-sided nonpaired t-test between DMSO and other treatments, exact P values are (from left to right bars) = 0.00015, 9.29×10^{-6} and 0.0017. **f**, Normalized SPARK in cells expressing various FAK variants. The cells co-expressed dominant-negative FAK (dnFAK) and FAK–SPARK, $n = 5$ biological replicates, two-sided nonpaired t-test between pcDNA and other treatments, exact P values are (from left to right bars) = 0.021, 3.34×10^{-5}, 0.034, 0.034 and 1.80×10^{-5}. Data are mean ± s.e.m. $^{*}P < 0.05$, $^{**}P < 0.01$ and $^{***}P < 0.001$. Scale bars, 1 μm (**a**), 10 μm (**d**) and 15 μm (**e**).

showed the accumulation of IFP2–paxillin signal and tension signal at the cell edge, confirming that FAs generated tension signal as noted in prior studies (Extended Data Fig. 6b)[39,44,45]. The FAK–SPARK channel also showed green droplets accumulated at the cell edge near integrin tension and paxillin recruitment (Extended Data Fig. 6b). Our previous studies and appropriate controls confirm that the tension signal indeed measures tension and does not result from some artifact at sites of integrin binding to the RGD–DNA substrate (Supplementary Fig. 14)[37,39] and that the tension signal does not result from spectral bleed-through between channels (Supplementary Fig. 14). To investigate the dynamics of FAK activation, we next collected time-lapse microscopy images in the tension, paxillin and FAK–SPARK channels and subjected them to kymograph analysis (Supplementary Fig. 15 and Supplementary Video 13). These videos identified newly forming adhesions as indicated by paxillin recruitment and appearance of tension. Interestingly, proximal FAK–SPARK droplets near the sites of FA formation and tension accumulation then appeared at a later timepoint (Extended Data Fig. 6c,d). The kymograph analysis was used (Extended Data Fig. 6c,e,f) to determine the temporal relationship between paxillin recruitment, FAK–SPARK activity and integrin tension (Methods). Briefly, we identified $t = 0$ min when tension puncta appeared and then recorded the time delay for the appearance of a FAK–SPARK signal. This analysis indicated an average delay time of 21.0 ± 9.0 min between initial tension recruitment and FAK–SPARK droplet formation. Interestingly, the time delay was nearly identical when the analysis was performed for paxillin recruitment and FAK–SPARK signal (Extended Data Fig. 6d,e). This temporal delay exceeds the measured delay of 1–2 min (Fig. 2f) between the onset of FAK phosphorylation and the appearance of the FAK–SPARK signal using CA–FAK. Thus, our data show that FAK phosphorylation occurs at the sites of FAs following the transmission of mechanical tension to integrins.

Next, to further investigate the causal relationship between integrin tension and FAK activation, we designed a set of experiments that controlled integrin force levels and then recorded FAK signaling outcomes. Specifically, we anchored the RGD ligands to the tension gauge tether (TGT), which is a double-stranded DNA duplex that dissociates

from the substrate at different magnitudes of force, described as the tension tolerance (T_{tol}; Fig. 6a and Supplementary Fig. 21)[42,46–48]. The T_{tol} can be tuned from ~12 pN to 56 pN by altering the geometry of the TGT. When the RGD ligand on the top strand is at the same end of the duplex as the anchoring group on the bottom strand, then forces lead to unzipping that is facile and requires ~12 pN of force. Conversely, when the RGD ligand is at the opposite end of the duplex compared to the surface anchoring group, then applied force re-orient the probe into a shearing geometry and dehybridization requires large forces of ~56 pN (Fig. 6a)[42,48]. The top and bottom strands are modified with quencher and fluorophore, respectively, such that mechanical denaturation of DNA is quantified by fluorescence (Fig. 6a). Conveniently, we used total internal reflectance fluorescence (TIRF) microscopy to map DNA dehybridization, which is a readout of traction force history.

HeLa cells transfected with FAK–SPARK and IFP2–paxillin were plated on TGT surfaces of 12 pN and 56 pN T_{tol} for 20 min, and then we imaged these three fluorescence channels in single cells to quantify FA formation, TGT rupture and FAK–SPARK signaling. Consistent with prior reports[46], cell spreading and FA formation were limited on the 12 pN probes, but the TGT signal was greater for these 12 pN probes. Interestingly, FAK–SPARK droplets were more abundant on 56 pN TGTs compared to 12 pN TGTs (Fig. 6b,c). We also found that while the FA area was approximately twofold smaller in cells seeded on 12 pN TGT substrate than those on 56 pN TGT, the FAK–SPARK activity normalized by FA area was higher in cells seeded on 56 pN TGT substrate than those on 12 pN TGT, demonstrating that FAK activity is proportional to the amplitude of the tension even when the activity is normalized to the FA area (Supplementary Fig. 22). This difference in activity was sustained over 80 min of cell spreading as quantified by image segmentation analysis (Supplementary Fig. 23; Methods) demonstrating the persistent influence of ligand T_{tol} on FAK activity. Time-lapse imaging of FAK–SPARK droplets showed retrograde flow for both 12 pN and 56 pN TGTs, and the differential FAK signaling and dynamics were sustained over 80 min of imaging (Supplementary Fig. 23 and Supplementary Videos 14 and 15). Moreover, we also quantified phospho-FAK Y397 levels for cells on 12 pN and 56 pN TGTs. These immunostaining experiments confirm the fidelity of the FAK–SPARK biosensor and showed substantially enhanced FAK pY397 signal per cell for the 56 pN TGT compared to that of the 12 pN probes (Supplementary Fig. 24; Methods). Increased FAK–SPARK activity for cells on 56 pN TGTs demonstrates that FAK activity is mechanosensitive and specifically integrin–ligand forces >12 pN lead to enhanced FAK signaling.

Discussion

Our phase separation-based FAK activity reporter FAK–SPARK has several advantages compared to previous FAK reporters[30,49,50]. First, FAK–SPARK achieves large dynamic range, simple signal pattern and high brightness, which enable robust detection of FAK activity in living cells and animals. As a comparison, previous genetically encoded FAK activity reporters such as FRET-based reporters have a small dynamic range due to weak fluorescence change of the donor and acceptor fluorophores upon FAK activation, which makes them difficult to detect FAK activation. Second, FAK–SPARK achieves a spatial resolution in single FAs and even within a single FA. This is consistent with another GFP phase separation-based reporter for imaging ATM kinase activity upon DNA damage[51,52]. In contrast, previous FAK reporters suffer from poor spatial resolution. For example, they require genetic targeting of FAs to detect FAK activity in FAs[30]. We emphasize that to achieve the spatial and temporal resolution of FAK activity, formation of FAK–SPARK droplets should be monitored because of the relatively long lifetime of the droplets and that they may drift away if there is intracellular fluid flow, such as actin retrograde flow. Third, FAK–SPARK reporter does not require exogenous expression of FAK, which is advantageous to the other reporters[49,50]. Fourth, FAK–SPARK achieves fast temporal resolution within 1–2 min based on the data with expression of active FAK in the nucleus, which enables detection of FAK activation dynamics during FA turnover including assembly and disassembly. On the other hand, the long time delay between tension build-up and FAK–SPARK signal suggests that the temporal resolution of FAK–SPARK likely depends on several factors, including the time for FAK activation and accumulation of sufficient FAK activity that leads to SPARK droplet formation. Taken together, FAK–SPARK provides an excellent tool for spatiotemporal imaging of FAK activity within single FAs in living cells and animals using appropriate imaging approaches.

Our data suggest that FAK is active where FAs are most dynamic including FA turnover (assembly and disassembly). Previous studies show that FAK enhances cell spreading[53]. Indeed, we observed that FAK activation follows FA assembly during cell spreading and migration and that FAK activation is proportional to cell spreading. We also found FAK activation during FA disassembly, suggesting that FAK activity is likely required for FA disassembly. This is consistent with previous studies that in FAK-deficient mice, cells show larger FAs, in addition to reduced cell motility[4]. FAK activation and potential phosphorylation of its substrate proteins in FA may trigger downstream events, resulting in FA disassembly. And FAK activation might be caused by tension resulted from the contraction of actin cytoskeleton.

The present study showed that FAK activity is polarized along the newly formed single FAs at the leading edge of a migrating cell. Interestingly, several previous studies suggest that FAK is a tension-activatable kinase and that the FERM domain of FAK interacts with and inhibits the kinase domain, and that tension-induced pulling dissociates the FERM from the kinase domain, initiating FAK activation[29,54–56]. Furthermore, a previous study reported that the traction force on single FAs is skewed to the distal tip of FAs (toward the leading edge)[57] and that paxillin is more phosphorylated at the distal tip[18].

Combining these with our observations, we propose a model to explain the observed polarization of FAK activity (Fig. 4h). In the leading edge of a migrating cell, actin and actomyosin contraction generates forces, which are likely stronger when closer to the membrane (Fig. 4h). Transmission of this actin contraction-generated force from actin cytoskeleton to FAK (via actin–vinculin–paxillin–FAK[26]) depends on the following: (1) interaction of FAK's FAT domain with paxillin within single FAs that are connected to actin filament; (2) the integrin–ECM interaction, which anchors the FAs to the substratum and (3) the FERM interaction with the plasma membrane via PI(4,5)P2 (refs.29,30). Combining these factors, the tension on FAK is likely stronger toward the leading edge, as shown by the previous observations of polarized tension within single FAs toward the leading edge[57]. This may lead to differential degree of FERM dissociation from the kinase, resulting in polarized FAK activities within single FAs, consistent with polarized paxillin phosphorylation[18]. On the other hand, FAK activity enhances actin polymerization via regulating Rho-family GTPases[58]. The polarized FAK activity may thus direct actin polymerization and contractibility via actomyosin, generating positive feedback with the actin contractibility-induced tension on FAK and its activation, resulting in membrane protrusion by actin polymerization and directed cell migration. Therefore, our results, together with previous studies, suggest that polarized tension and FAK activity in single FAs at the leading edge may guide cell migration.

To support the proposed model, we conducted various studies including mutagenesis and DNA tension probe-based approaches. We showed that the FAK activity we observed does depend on integrin because inhibition of integrin by small molecule inhibitors of α5β1 or antibodies against α5 abolished FAK activity. Second, inhibitors of actin polymerization, myosin II and Rho-associated protein kinase (ROCK), reduce FAK activity. These data indicate that FAK activation does depend on the actin cytoskeleton. Our results are consistent with the current consensus that the actin cytoskeleton propagates force to FAs via FA connection with actin filament and integrin[18]. We also verified that FAK activity is dependent on the FERM domain's interaction with PI(4,5)

https://doi.org/10.1038/s41589-023-01353-y

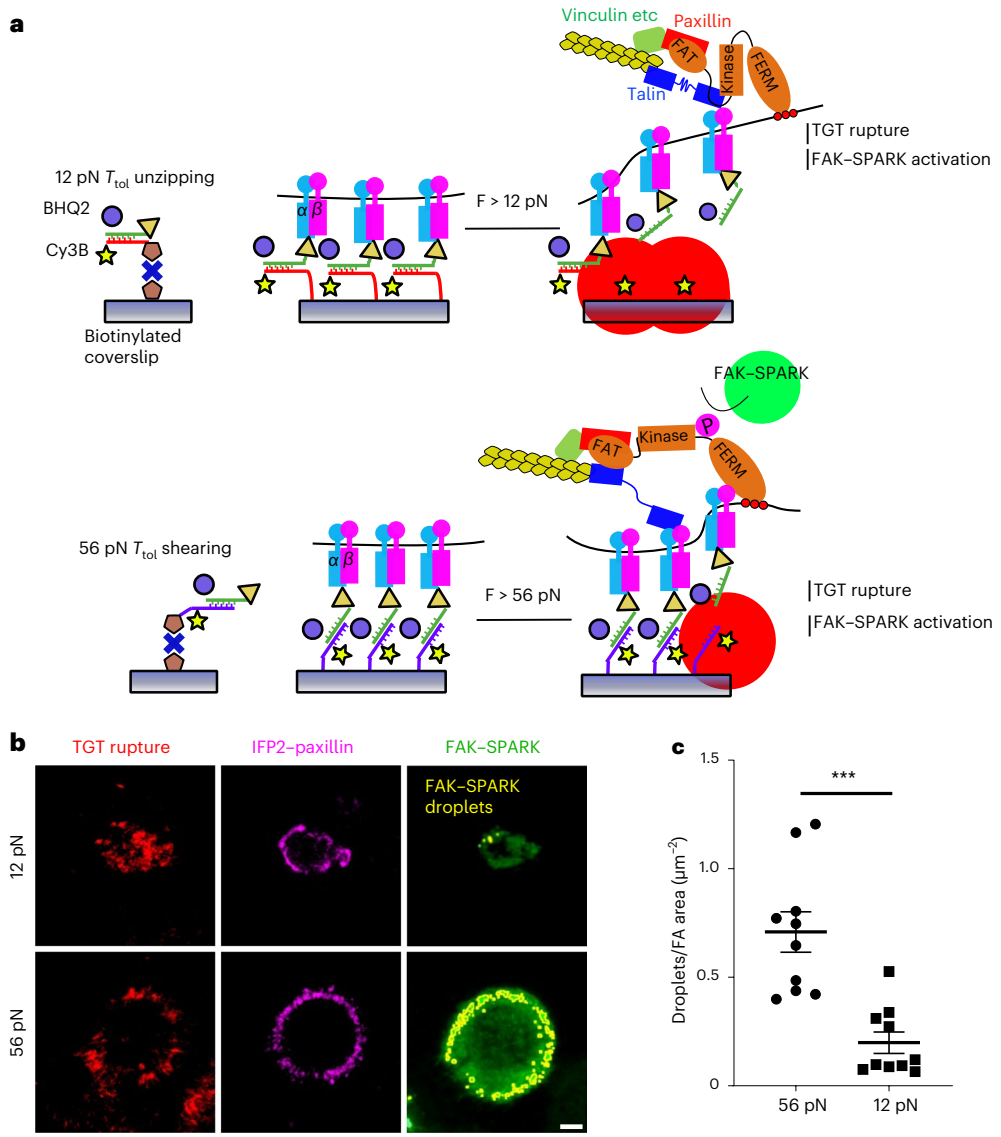

Fig. 6 | FAK–SPARK droplet formation scales with integrin ligand T_{tol}. a, Diagram of 12 pN TGT geometry and TGT force induced fluorescence and FAK activation mechanism. **b**, FAK–SPARK droplet (green outlined in yellow) fluorescence micrographs of HeLa cells transfected with FAK–SPARK and on 12 pN and 56 pN TGTs after 30 min incubation. This experiment was repeated four times independently with similar results. **c**, Number of identified FAK–SPARK droplets normalized by FA area in each cell for 12 pN and 56 pN TGTs. $n = 10$ cells (four biological replicates), two-sided nonpaired t-test, $P = 0.0003$. Data are mean ± s.e.m. ***$P < 0.001$. Scale bar, 5 μm (**b**).

P2 because disruption of FERM::PI(4,5)P2 interaction by mutagenesis does reduce FAK activity. And we further showed that FAK inhibition is dependent on the FERM domain's association with the kinase domain of FAK because the reduction of this interaction by mutating key residues that mediate this interaction increases FAK activity.

It is currently debated as to whether integrin-mediated traction force is directly sensed by FAK and triggers its activation, or whether FAK signaling exclusively promotes the generation of integrin traction forces. For example, it is thought that substrate stiffness does not affect the rate at which FAK is recruited to FAs[59]. It was hypothesized that allosteric changes induced by cell membrane interactions are responsible for the priming of FAK, which fits with a model where FAK activation occurs by force[60]. Furthermore, multiple studies support the model that FAK is a mechanosensor. FAK undergoes changes in autophosphorylation in response to changing substrate stiffness for FN-coated surfaces[30]. Micropillar array deflection experiments showed that inhibition of FAK reduces FA paxillin phosphorylation, vinculin recruitment and integrin-mediated traction force on FN substrates, demonstrating that FAK has a downstream influence on FA traction force[61]. Recent single-molecule force spectroscopy measurements showed that FERM-kinase rupture is associated with a force peak, suggesting that FAK kinase activity could be modulated by mechanical tension because the FERM domain is known to inhibit the kinase activity and its dissociation could lead to kinase activation[62]. Perhaps the strongest evidence to support that FAK is a mechanosensor comes from a study[63] showing that FAK phosphorylation (pY397) and total FAK correlate with the amplitude of the applied force.

Our results strongly support that FAK is a mechanosensor that detects piconewton integrin force magnitude. Although we do not provide evidence of the mechanism of mechanosensation, the literature suggests that forces drive a conformational change of FAK out of the autoinhibited state, which is akin to the mechanism of how vinculin senses tension within FAs. Our data demonstrate that FAK activation occurs within FAs in less than 20 min following the mounting of tension

and recruitment of FA markers. Moreover, capping the forces at FAs using the TGT to values <12 pN shows dampening of FAK activity, thus directly demonstrating a causal link between integrin tension and FAK activity. Taken together, our data are consistent with a model where FAK directly senses integrin tension and responds by phosphorylation of its kinase.

Online content

Any methods, additional references, Nature Portfolio reporting summaries, source data, extended data, supplementary information, acknowledgements, peer review information; details of author contributions and competing interests; and statements of data and code availability are available at https://doi.org/10.1038/s41589-023-01353-y.

References

1. Kechagia, J. Z., Ivaska, J. & Roca-Cusachs, P. Integrins as biomechanical sensors of the microenvironment. *Nat. Rev. Mol. Cell Biol.* **20**, 457–473 (2019).
2. Burridge, K. Focal adhesions: a personal perspective on a half century of progress. *FEBS J.* **284**, 3355–3361 (2017).
3. Mitra, S. K., Hanson, D. A. & Schlaepfer, D. D. Focal adhesion kinase: in command and control of cell motility. *Nat. Rev. Mol. Cell Biol.* **6**, 56–68 (2005).
4. Ilic, D. et al. Reduced cell motility and enhanced focal adhesion contact formation in cells from FAK-deficient mice. *Nature* **377**, 539–544 (1995).
5. Parsons, J. T., Horwitz, A. R. & Schwartz, M. A. Cell adhesion: integrating cytoskeletal dynamics and cellular tension. *Nat. Rev. Mol. Cell Biol.* **11**, 633–643 (2010).
6. Seong, J. et al. Detection of focal adhesion kinase activation at membrane microdomains by fluorescence resonance energy transfer. *Nat. Commun.* **2**, 406 (2011).
7. Chung, C.-I., Zhang, Q. & Shu, X. Dynamic imaging of small molecule induced protein–protein interactions in living cells with a fluorophore phase transition based approach. *Anal. Chem.* **90**, 14287–14293 (2018).
8. Zhang, Q. et al. Visualizing dynamics of cell signaling in vivo with a phase separation-based kinase reporter. *Mol. Cell* **69**, 334–345.e5 (2018).
9. Schepis, A. et al. Protease signaling regulates apical cell extrusion, cell contacts, and proliferation in epithelia. *J. Cell Biol.* **217**, 1097–1112 (2018).
10. Zouq, N. K. et al. FAK engages multiple pathways to maintain survival of fibroblasts and epithelia: differential roles for paxillin and p130Cas. *J. Cell Sci.* **122**, 357–367 (2009).
11. Mastop, M. et al. Characterization of a spectrally diverse set of fluorescent proteins as FRET acceptors for mTurquoise2. *Sci. Rep.* **20**, 11999 (2017).
12. Tsutsui, H., Karasawa, S., Okamura, Y. & Miyawaki, A. Improving membrane voltage measurements using FRET with new fluorescent proteins. *Nat. Methods* **5**, 683–685 (2008).
13. Yu, D. et al. Rational design of a monomeric and photostable far-red fluorescent protein for fluorescence imaging in vivo. *Protein Sci.* **25**, 308–315 (2015).
14. Yu, D. et al. A naturally monomeric infrared fluorescent protein for protein labeling. *Nat. Methods* **12**, 763–765 (2015).
15. Yu, D. et al. An improved monomeric infrared fluorescent protein for neuronal and tumour brain imaging. *Nat. Commun.* **5**, 3626 (2014).
16. Shu, X. et al. Mammalian expression of infrared fluorescent proteins engineered from a bacterial phytochrome. *Science* **324**, 804–807 (2009).
17. Banaszynski, L. A., Liu, C. W. & Wandless, T. J. Characterization of the FKBP.rapamycin.FRB ternary complex. *J. Am. Chem. Soc.* **127**, 4715–4721 (2005).
18. Case, L. B. & Waterman, C. M. Integration of actin dynamics and cell adhesion by a three-dimensional, mechanosensitive molecular clutch. *Nat. Cell Biol.* **17**, 955–963 (2015).
19. McGrath, J. L. Cell spreading: the power to simplify. *Curr. Biol.* **17**, R357–R358 (2007).
20. Tomar, A., Lim, S.-T., Lim, Y. & Schlaepfer, D. D. A FAK-p120RasGAP-p190RhoGAP complex regulates polarity in migrating cells. *J. Cell Sci.* **122**, 1852–1862 (2009).
21. Ezratty, E. J., Partridge, M. A. & Gundersen, G. G. Microtubule-induced focal adhesion disassembly is mediated by dynamin and focal adhesion kinase. *Nat. Cell Biol.* **7**, 581–590 (2005).
22. Ballestrem, C., Hinz, B., Imhof, B. A. & Wehrle-Haller, B. Marching at the front and dragging behind. *J. Cell Biol.* **155**, 1319–1332 (2001).
23. Laukaitis, C. M., Webb, D. J., Donais, K. & Horwitz, A. F. Differential dynamics of alpha 5 integrin, paxillin, and alpha-actinin during formation and disassembly of adhesions in migrating cells. *J. Cell Biol.* **153**, 1427–1440 (2001).
24. Gardel, M. L. et al. Traction stress in focal adhesions correlates biphasically with actin retrograde flow speed. *J. Cell Biol.* **183**, 999–1005 (2008).
25. Feliks, M., Lafaye, C., Shu, X., Royant, A. & Field, M. Structural determinants of improved fluorescence in a family of bacteriophytochrome-based infrared fluorescent proteins: insights from continuum electrostatic calculations and molecular dynamics simulations. *Biochemistry* **55**, 4263–4274 (2016).
26. Le Coq, J., Acebrón, I., Rodrigo Martin, B., López Navajas, P. & Lietha, D. New insights into FAK structure and function in focal adhesions. *J. Cell Sci.* **135**, jcs259089 (2022).
27. Swaminathan, V., Fischer, R. S. & Waterman, C. M. The FAK-Arp2/3 interaction promotes leading edge advance and haptosensing by coupling nascent adhesions to lamellipodia actin. *Mol. Biol. Cell* **27**, 1085–1100 (2016).
28. Serrels, B. et al. Focal adhesion kinase controls actin assembly via a FERM-mediated interaction with the Arp2/3 complex. *Nat. Cell Biol.* **9**, 1046–1056 (2007).
29. Goñi, G. M. et al. Phosphatidylinositol 4,5-bisphosphate triggers activation of focal adhesion kinase by inducing clustering and conformational changes. *Proc. Natl Acad. Sci. USA* **111**, E3177–E3186 (2014).
30. Seong, J. et al. Distinct biophysical mechanisms of focal adhesion kinase mechanoactivation by different extracellular matrix proteins. *Proc. Natl Acad. Sci. USA* **110**, 19372–19377 (2013).
31. Orgovan, N. et al. Dependence of cancer cell adhesion kinetics on integrin ligand surface density measured by a high-throughput label-free resonant waveguide grating biosensor. *Sci. Rep.* **4**, 4034 (2014).
32. Sundaram, A. et al. Targeting integrin α5β1 ameliorates severe airway hyperresponsiveness in experimental asthma. *J. Clin. Invest.* **127**, 365–374 (2017).
33. Pasapera, A. M., Schneider, I. C., Rericha, E., Schlaepfer, D. D. & Waterman, C. M. Myosin II activity regulates vinculin recruitment to focal adhesions through FAK-mediated paxillin phosphorylation. *J. Cell Biol.* **188**, 877–890 (2010).
34. Labouesse, C., Verkhovsky, A. B., Meister, J.-J., Gabella, C. & Vianay, B. Cell shape dynamics reveal balance of elasticity and contractility in peripheral arcs. *Biophys. J.* **108**, 2437–2447 (2015).
35. Petridou, N. I., Stylianou, P. & Skourides, P. A. A dominant-negative provides new insights into FAK regulation and function in early embryonic morphogenesis. *Development* **140**, 4266–4276 (2013).
36. Zheng, Y. et al. FAK phosphorylation by ERK primes Ras-induced tyrosine dephosphorylation of FAK mediated by PIN1 and PTP-PEST. *Mol. Cell* **35**, 11–25 (2009).

37. Blanchard, A. et al. Turn-key mapping of cell receptor force orientation and magnitude using a commercial structured illumination microscope. *Nat. Commun.* **12**, 4693 (2021).
38. Glazier, R., Shinde, P., Ogasawara, H. & Salaita, K. Spectroscopic analysis of a library of DNA tension probes for mapping cellular forces at fluid interfaces. *ACS Appl. Mater. Interfaces* **13**, 2145–2164 (2021).
39. Glazier, R. et al. DNA mechanotechnology reveals that integrin receptors apply pN forces in podosomes on fluid substrates. *Nat. Commun.* **10**, 4507 (2019).
40. Stabley, D. R., Jurchenko, C., Marshall, S. S. & Salaita, K. S. Visualizing mechanical tension across membrane receptors with a fluorescent sensor. *Nat. Methods* **9**, 64–67 (2011).
41. Zhang, Y. et al. Platelet integrins exhibit anisotropic mechano-sensing and harness piconewton forces to mediate platelet aggregation. *Proc. Natl Acad. Sci. USA* **115**, 325–330 (2018).
42. Wang, X. & Ha, T. Defining single molecular forces required to activate integrin and notch signaling. *Science* **340**, 991–994 (2013).
43. Pfaff, M. et al. Selective recognition of cyclic RGD peptides of NMR defined conformation by αIIbβ3, αVβ3, and α5β1 integrins. *J. Biol. Chem.* **269**, 20233–20238 (1994).
44. Liu, Y. et al. Nanoparticle tension probes patterned at the nanoscale: impact of integrin clustering on force transmission. *Nano Lett.* **14**, 5539–5546 (2014).
45. Liu, Y., Yehl, K., Narui, Y. & Salaita, K. Tension sensing nanoparticles for mechano-imaging at the living/nonliving interface. *J. Am. Chem. Soc.* **135**, 5320–5323 (2013).
46. Rashid, S. A. et al. DNA tension probes show that cardiomyocyte maturation is sensitive to the piconewton traction forces transmitted by integrins. *ACS Nano* **16**, 5335–5348 (2022).
47. Pérez, L. A. et al. An outside-in switch in integrin signaling caused by chemical and mechanical signals in reactive astrocytes. *Front. Cell Dev. Biol.* **9**, 712627 (2021).
48. Jo, M. H., Cottle, W. T. & Ha, T. Real-time measurement of molecular tension during cell adhesion and migration using multiplexed differential analysis of tension gauge tethers. *ACS Biomater. Sci. Eng.* **5**, 3856–3863 (2019).
49. Ritt, M., Guan, J.-L. & Sivaramakrishnan, S. Visualizing and manipulating focal adhesion kinase regulation in live cells. *J. Biol. Chem.* **288**, 8875–8886 (2013).
50. Cai, X. et al. Spatial and temporal regulation of focal adhesion kinase activity in living cells. *Mol. Cell. Biol.* **28**, 201–214 (2008).
51. Li, X. et al. ATM-SPARK: a GFP phase separation-based activity reporter of ATM. *Sci. Adv.* **9**, eade3760 (2023).
52. Shu, X. Imaging dynamic cell signaling in vivo with new classes of fluorescent reporters. *Curr. Opin. Chem. Biol.* **54**, 1–9 (2020).
53. Wakatsuki, T., Wysolmerski, R. B. & Elson, E. L. Mechanics of cell spreading: role of myosin II. *J. Cell Sci.* **116**, 1617–1625 (2003).
54. Bell, S. & Terentjev, E. M. Focal adhesion kinase: the reversible molecular mechanosensor. *Biophys. J.* **112**, 2439–2450 (2017).
55. Zhou, J. et al. Mechanism of focal adhesion kinase mechanosensing. *PLoS Comput. Biol.* **11**, e1004593 (2015).
56. Zhou, J., Bronowska, A., Le Coq, J., Lietha, D. & Gräter, F. Allosteric regulation of focal adhesion kinase by PIP2 and ATP. *Biophys. J.* **108**, 698–705 (2015).
57. Plotnikov, S. V., Pasapera, A. M., Sabass, B. & Waterman, C. M. Force fluctuations within focal adhesions mediate ECM-rigidity sensing to guide directed cell migration. *Cell* **151**, 1513–1527 (2012).
58. Pollard, T. D. & Cooper, J. A. Actin, a central player in cell shape and movement. *Science* **326**, 1208–1212 (2009).
59. Stutchbury, B., Atherton, P., Tsang, R., Wang, D.-Y. & Ballestrem, C. Distinct focal adhesion protein modules control different aspects of mechanotransduction. *J. Cell Sci.* **130**, 1612–1624 (2017).
60. Acebrón, I. et al. Structural basis of focal adhesion kinase activation on lipid membranes. *EMBO J.* **39**, e104743 (2020).
61. Panagiotakopoulou, M. et al. Cell cycle-dependent force transmission in cancer cells. *Mol. Biol. Cell* **29**, 2528–2539 (2018).
62. Bauer, M. S. et al. Structural and mechanistic insights into mechanoactivation of focal adhesion kinase. *Proc. Natl Acad. Sci. USA* **116**, 6766–6774 (2019).
63. Zhou, D. W. et al. Force-FAK signaling coupling at individual focal adhesions coordinates mechanosensing and microtissue repair. *Nat. Commun.* **12**, 2359 (2021).

Methods

Plasmid construction and lentivirus production

All plasmid constructs were created and purified by standard molecular biology techniques and confirmed by exhaustively sequencing the cloned fragments. To create FAK–SPARK, DNA fragments encoding ETDD**Y**AEIIDE were inserted to replace FKBP in the pcDNA3 FKBP–EGFP–HOTag3 construct[7,8]. DNA sequence encoding SH2 domain was inserted upstream of a nonfluorescent variant of GFP (EGFP* containing Y66F mutation) followed by HOTag6. A 'self-cleaving' 2A (T2A) sequence was further added to 3′-downstream of FAK–EGFP–HOTag3 via PCR, and the resulting FAK–EGFR–HOTag3–T2A fragment was then subcloned into 5′-upstream of SH2–EGFP*–HOTag6 to generate the full FAK–SPARK expressing vector. The tyrosine was changed to phenylalanine (ETDD-**P**AEIIDE) for the mutFAK–SPARK via designed DNA oligo-synthesis. FAK–SPARK–NLS was generated via inserting the NLS sequence (PAAKRVKLD) before EGFP and EGFP* in FAK–SPARK. For the lentiviral vector, the DNA fragment encoding FAK–SPARK was cloned into pHR–SFFV–GFP1-10 (GFP1-10 fragment) to replace GFP1-10. Lentivirus production followed the standard protocol of 'Improve Lentiviral Production Using Lipofectamine 3000 Reagent' from Thermo Fisher Scientific.

Cell culture

The HEK293, 293FT, HeLa, U2OS, MDA–MB-231 and MEF cells were passaged in Dulbecco's modified Eagle medium, while Kelly and SHEP cells were passaged in Roswell Park Memorial Institute (RPMI)-1640 medium supplemented with 10% FBS, nonessential amino acids, penicillin (100 units per ml) and streptomycin (100 μg ml^{-1}). All culture supplies were obtained from the University of California San Francisco Cell Culture Facility.

Live cell imaging

Cells were grown on Nunc Lab-Tek II chambered coverglass for imaging experiment. To express FAK–SPARK, HEK293 cells were transiently transfected using calcium phosphate transfection reagent with 50 ng FAK–SPARK plasmid. HeLa cells were transiently transfected using Lipofectamine 3000 transfection reagent with 100 ng FAK–SPARK and 50 ng paxillin–mApple. HEK293 and HeLa cell were imaged 1 d after transfection. U2OS, MDA–MB-231, Kelly, SHEP, SKNAS and MEF cells were infected with a medium containing ATM–SPARK lentivirus and imaged 3 d after infection.

All imaging was carried out on Nikon Eclipse Ti inverted microscope equipped with Yokogawa CSU-W1 confocal scanner unit (Andor), digital complementary metal oxide semiconductor camera ORCA-Flash4.0 (Hamamatsu) and ASI MS-2000 XYZ automated stage (Applied Scientific Instrumentation). Imaging was performed in the environmental control unit incubation chamber (In Vivo Scientific) maintained at 37 °C and with 5% CO_2. Fluorescence images were acquired using Nikon CFI Plan Apochromatic ×20 dry (numerical aperture (NA): 0.75) objective or CFI apochromatic TIRF ×60 oil objective (NA: 1.49) against GFP, Cherry and IFP per experiment settings.

HeLa cell transfection and reseeding

HeLa cells (~80% confluency in a 24-well plate) were transfected with pcDNA–FAK–SPARK (1 μg) and paxillin–mApple (0.2 μg) or paxillin–mApple-–CA–FAK or paxillin–IFP2 with lipofectamine. Five hours later, the medium was changed with fresh. Prepare FN-coated image chamber by incubating the chamber with 10 μg ml^{-1} FN at 37° for 1 h followed by 3× PBS washing. Twenty-four hours after transfection, transfected HeLa cells were resuspended with 0.05% trypsin, then washed and collected in a CO_2-independent medium (with 10% FBS). After incubation, cells were checked for time-lapse imaging. For drug treatment during reseeding, 1652 (dual inhibitor of α5β1 and αvβ1), P1D6 (anti-integrin α5 antibody), cytochalasin D, blebbistatin and Y27632 were added together with resuspended cells into FN-coated chamber and imaged for FAKS–SPARK signal at an indicated time with a microscope. In total, 1 μM biliverdin was added for imaging with IFP2 (FAK–SPARK/tension probe experiments).

Generation of FAK knockdown HeLa cell line

Lentiviral vector with shRNA for targeting human FAK (CCGATTGGAAACCAACATATA) was a generous gift from V. Weaver. Lentivirus was produced and used to infect HeLa cells. After puromycin selection, cells were maintained for further use.

Zebrafish maintenance and imaging

Zebrafish were maintained and handled in compliance with the standard protocols (http://zfin.org) and the University of California San Francisco Institutional Animal Care and Use Committee protocols. WT strains used were EKW. UAS–FAK–SPARK and UAS–mutSPARK transgenic zebrafish were made with Tol2 system. UAS-zebrafish were mated with TgBAC (ΔNp63:Gal4FF)^{la213} for skin expression. Imaging was carried out 2 d postfertilization (2 dpf) using Nikon Eclipse Ti inverted microscope under ×20 objective.

Phospho-FAK Y397 immunofluorescence microscopy

HeLa cells were incubated for 90 min on TGT surfaces in a full culture medium. Then, the medium was removed and replaced with 4% (vol/vol) formaldehyde in PBS and incubated for 15 min to allow fixation. Special care was taken to reduce the force fluid shear flow during wash steps so as not to dissociate adhered cells from the surface. Formaldehyde solution was then removed, surfaces were washed with three well volumes of PBS and then incubated with 0.1% (vol/vol) Triton-X in PBS, washed again, then incubated in 100 mg ml^{-1} bovine serum albumin (BSA) for 1 h. Cells were then incubated in 1 μg ml^{-1} anti-FAK (phospho Y397) antibody EP2160Y in PBS, rabbit monoclonal (Abcam, ab81298) for 12 h at 4 °C. Cells were then washed with PBS and stained with 3 μg ml^{-1} goat antirabbit IgG Alexa Fluor-488 (Abcam, ab150077) in PBS and 50 μl nuc-blue (Invitrogen, R3760; to confirm cell presence via nuclear stain) in PBS for 1 h and then imaged.

Mass spectrometry (MS)

For synthetic intermediates products (products 1 and 2; Supplementary Fig. 4), matrix-assisted laser deabsorption ionization (MALDI) time-of-flight (TOF) MS was carried out on an Applied Biosystems 4700 Proteomics Analyzer MALDI–TOF mass spectrometer by dissolving the oligonucleotide at a concentration of 0.1–20 μM in a saturated solution of 3-hydroxypicolinic acid dissolved in of 49.4% (vol/vol) acetonitrile, 0.1% trifluoroacetic acid and 49.4% water; 5 mg ml^{-1} ammonium citrate or saturated solution of α-cyano-4-hydroxycinnamic acid in 49.4% (vol/vol) H_2O, 49.4% acetonitrile and 0.1% trifluoroacetic acid. For synthetic products 3–6 (Supplementary Fig. 4), the molecular weight of the products was evaluated with an electrospray ionization method using a Thermo Fisher Scientific LTQ Orbitrap. The samples were prepared in the mixture of 70% (18.2 MΩ) nanopure water and 30% methanol containing 10 μM ethylenediaminetetraacetic acid, 0.0375% triethylamine and 0.75% of 1,1,1,3,3,3-hexafluoro-2-propanol and recorded the spectra with negative charge mode eluted with the same solution. The main peak of obtained electrospray ionization–MS spectrum (m/z) was then deconvoluted to obtain the average molecular weight for the oligonucleotides[64].

DNA strand hybridization

To anneal MTFM and TGT DNA strands, the respective oligonucleotides were suspended in 20 μl PBS at a concentration of 1 μM in a 0.2-ml microcentrifuge tube. Oligonucleotides were denatured at 95 °C for 5 min and subsequently annealed by returning to 25 °C at a rate of 1.3 °C min^{-1}.

Fabrication of 19 pN hairpin MTFM surfaces and imaging

Modified DNA strands were purchased from Integrated DNA Technologies and functionalized as previously reported (Supplementary Table 1

and Supplementary Fig. 13)[65]. To prepare MTFM probe-modified coverslips, 25 mm no. 2 diameter borosilicate glass coverslips (VWRCIR2-25MM) were mounted on a fluorocarbon rack in a 40 ml beaker and rinsed three times in 40 ml of ethanol. Coverslips were then sonicated in ethanol for 30 min and then dried in an oven at 100 °C for 20 min. Surfaces were then functionalized with biotin, streptavidin and then an MTFM probe (Supplementary Fig. 13). The cleaned slides were treated with fresh piranha solution (3:1 vol/vol H_2SO_4:H_2O_2) for 10 min. CAUTION: piranha solution is highly corrosive and may violently explode if mixed with organic solvents. The coverslips were then rinsed six times with 40 ml of 18.2 MΩ resistance purity (nanopure) water and three times with pure ethanol. Subsequently, slides were incubated in a solution of 3% (vol/vol) (3-aminopropyl)triethoxysilane (Sigma, 440140-100ML) solution in ethanol for 1 h. Then, the coverslips were washed 3× with ethanol and dried in an oven at 100 °C for 30 min. The dry coverslips were then incubated overnight with 2 mg ml^{-1} NHS-biotin (Thermo Fisher Scientific, 20217) in anhydrous DMSO in a petri dish at room temperature sealed with parafilm. Biotin-modified coverslips were stored at 4 °C and used within 2 weeks of preparation. On the day of FAK–SPARK/tension probe experiments, substrates were rinsed with ethanol, mounted in an Attofluor cell chamber (Thermo Fisher Scientific, A7816) for microscopy and washed with 3 × 1 ml chamber volumes of PBS (pH 7.4). The mounted surfaces were incubated with 0.1% BSA in PBS for 30 min, washed with 3 ml PBS and then covered with a 50 μg ml^{-1} solution of streptavidin (Rockland, S000-01) in PBS. After incubating the coverslips for 1 h at room temperature, they were rinsed with 3 ml of PBS to remove the unbound streptavidin. The surfaces were then covered with 0.5 ml of 60 nM annealed MTFM probe DNA in PBS for 1 h. Unbound DNA was washed away with 3 ml PBS and 2 ml of normal culture media before plating cells on the surfaces.

Our previous studies demonstrated that the tension signal indeed measures tension and does not result from some artifact at sites of integrin binding to the RGD–DNA substrate. First, our previous study showed that the sensor is evenly distributed by generating probes that lack the quencher with a ±7% coefficient of variation[37,65]. Second, tension signal shows high coincidence with various FA markers (Supplementary Fig. 14)[65,66]. Furthermore, there are areas where adhesions form, but no significant tension has been built up (Supplementary Fig. 14; paxillin signal is high but without tension). Thus, tension signal does not result from spectral bleed-through between channels despite the high level of colocalization between tension and paxillin.

Fabrication of 12 pN and 56 pN TGT surfaces

TGTs of 12 pN and 56 pN were synthesized (Supplementary Figs. 15–21)[47]. Glass coverslips were cleaned with piranha solution as above for 30 min and washed with six volumes of nanopure water. Then coverslips were etched in 0.5 M KOH on ice in a sonicator for 30 min. Slides were then washed with six volumes of water and then four volumes of ethanol. Coverslips were then dried at 90 °C in an oven for 5 min. To reduce nonspecific binding of cells to surfaces, 150 mg ml^{-1} biotin–PEG–silane (molecular weight (MW) 5 kDa; Broadpharm, BP-24037) in anhydrous DMSO was added to the coverslips and baked at 90 °C in a glass Petri dish for 15 min[67]. Coverslips were then washed with three volumes of nanopure water, dried under a stream of nitrogen gas, stored at 4 °C and used within 2 weeks of fabrication. To functionalize surfaces with TGTs, the protocol for MTFM probes was followed as above but without blocking with BSA. TGT DNA probes were annealed as described above using the synthesized TGT DNA strands. Each replicate cell was plated and imaged in a 96-well round bottom microtiter plate (Grace Bio Labs, 204969) with functionalized coverslips applied to the adhesive bottom. Calculation of $F_{1/2}$ of DNA hairpin is outlined in Supplementary Fig. 12. The $F_{1/2}$ threshold at which the DNA hairpins have a 50% probability of unfolding and generating MTFM fluorescence signal is based on assumptions and measurements discussed in ref. 68.

Microscopy

Cells were seeded onto functionalized coverslips at a density of 2–3,000 cells per cm^2 and incubated at 37 °C in a 5% CO_2 atmosphere for 20–30 min before fluorescence microscopy imaging. Fluorescence microscopy was carried out using a Nikon Eclipse Ti driven by the NIS Elements Advanced Research software. The microscope objective used was CFI Apo ×100 (NA: 1.49) objective (Nikon). The optical system includes a TIRF variable mirror launcher and a Nikon Perfect Focus System, an interferometry-based device that corrects the z-drift of the stage. Fluorescence excitation of samples through the optical system was carried out with 488 nm (50 mW) and 561 nm (50 mW) lasers. Fluorescence micrographs of IFP2–paxillin were acquired using a light emitting diode source passed through a Cy5 fluorescence filter cube (Chroma 49006 filter set). The camera used to collect images was an Andor DU-897 X-9319 camera imaging at 50–500 ms exposure times. FLIM images were acquired using a Nikon Ti Eclipse Inverted Laser Scanning confocal microscope with a Plan Apo Lambda ×60/1.40 oil objective equipped with PicoQuant time-correlated single photon counting (TCSPC) upgraded with SymPhoTime 64 2.1.3813 TCSPC. The average fluorescence lifetime per pixel was determined using the SymPhoTime Fast FLIM algorithm.

FAK–SPARK particle delay time quantification

Fluorescence microscopy time-lapse videos of the FAK–SPARK and IFP2–paxillin transfected cells plated to 19 pN hairpin MTFM surfaces were collected. Newly forming adhesions of 19 pN fluorescence tension signal region of interests were manually selected for line-scan analysis using the Fiji ImageJ software package (NIH). Each line scan includes the newly formed 19 pN tension area in the early timepoint as well as the FAK–SPARK droplet forming in the later timepoint and averages a two pixels width along the direction in the line. Orientation of the line scan is positioned to include both tension-defined FA and FAK–SPARK droplet at the timepoint of the initial appearance of both FA and droplet, and also the droplet and tension area is closer than 2.5 μm in distance (Extended Data Fig. 6a). Images were then subjected to rolling ball background subtraction with a ball radius of 50 pixels to increase contrast and minimize background noise. Kymographs of the line scans were then generated with length on the *y* axis, time on the *x* axis and kymograph pixel intensity, the average pixel intensity, of the 2-pixel width of the linear ROI (Extended Data Fig. 6b). Individual kymographs of FAK–SPARK, tension and paxillin were generated and processed using a python script with the Anaconda package manager. The maximum intensity on the *y* axis (distance) of the kymograph is then plotted versus the *x* axis (time) of the kymograph (Extended Data Fig. 6c). The maximum intensity values of the plot of tension, FAK–SPARK and IFP2–paxillin are then normalized to a scale of 0–1. The time delay is calculated by subtracting the point on the FAK–SPARK trace where the normalized maximum intensity reaches 75% of its maximum value from that of the tension signal.

FAK–SPARK droplet production quantification

To quantify relative FAK–SPARK droplet production on TGTs, an algorithm using the Fiji ImageJ software package assisted by a macro script was used. Time-lapse micrographs of TIRF488 fluorescence were captured to track FAK–SPARK droplet production using 200 ms exposure time with 100% laser intensity settings every 30 s for 50 min (Supplementary Videos 13–15).

These were subjected to primary background subtracted subtracting half of the median pixel intensity value of the image frame from each frame. Each frame was then subjected to rolling ball background subtraction with a radius of 15 pixels. Timelapses were then corrected for stage drift using the Selective Plane Illumination Microscopy registration[69] ImageJ plugin and by selecting regions of immobile fluorescence intensity to generate an image a drift-corrected image. A manual pixel intensity threshold was then applied then the 'convert to mask'

function was applied to create a binary mask image of regions above the threshold intensity. The watershed image segmentation algorithm was applied as described below followed by the 'analyze particles' image segmentation function with a maximum particle area threshold that was varied as described below. The number of identified particles for each frame was then recorded.

To verify that the identified number of FAK–SPARK droplets identified by particle analysis over time does not change drastically for cells for 12 pN and 56 pN TGT. Three permutations of the droplet identification algorithm were employed. One with a low 8 μm^2 maximum particle area threshold without applying the watershed image segmentation operation (settings 1) to the binary mask image resulting from intensity thresholding, one with an 8 μm^2 maximum area and applying the watershed function (settings 2) and a third using a higher 24 μm^2 maximum particle area (settings 3). Modifying the particle identification algorithm settings changed the number of particles identified for some FAK–SPARK TIRF fluorescent micrographs (Supplementary Fig. 8). We found that FAK–SPARK droplet count did not change substantially for cells over time regardless of the droplet identification algorithm (Supplementary Fig. 8) through comparing the number of droplets produced using setting by the unpaired *t*-test with Welch's correction.

Phospho-FAK Y397 fluorescence quantification

To measure cell spread area, the RICM outline of the cell was manually created by creating an ROI of the cell edge and measuring its area. For measurements of fluorescence intensity, cell micrographs were subjected to background subtraction, bleed-through of fluorescence dye correction and camera detector background subtraction using a Python script. To measure TGT fluorescence, the signal intensity in the average intensity in the RICM ROI in the 561 nm channel was measured. To measure phospho-FAK Y397 fluorescence intensity, the average intensity in the 488 nm channel was measured within the RICM ROI was measured.

Western blot

Cells were washed three times in cold PBS and lysed in 1× lysis buffer (with protease inhibitor and phosphatase inhibitor added) after drug treatment. The lysate was further incubated at 4 °C for 40 min and centrifuged at 15,000*g* at 4 °C for 20 min. Supernatant was collected and mixed with NuPAGE LDS sample buffer (4×). Sample was further resolved in NuPAGE 4–12% Bis–Tris protein gels. After transferring, the membrane was blocked in PBST containing 5% nonfat milk and incubated with first antibodies (anti-pFAK EP2160Y; Abcam, ab81298 or anti-FAK antibody; Cell Signaling Technology, 3285; both 600× dilution) at 4 °C overnight. On the following day, membrane was washed three times in PBST and then incubated in horseradish peroxidase-conjugated second antibodies (1:1,000) for 1 h at room temperature. After washing three times with PBST, signal was visualized using standard enhanced chemiluminescence substrate on film. Blots were quantified with ImageJ.

Statistics

All data were processed with ImageJ (1.53q), GraphPad Prism 8.0, Microsoft Excel (v2208) and the SymPhoTime Fast FLIM algorithm.

Reporting summary

Further information on research design is available in the Nature Portfolio Reporting Summary linked to this article.

Data availability

All data are available in the article, including the source data section. Source data are provided with this paper.

References

64. Hail, M. E., Elliott, B. & Anderson, K. High-throughput analysis of oligonucleotides using automated electrospray ionization mass spectrometry. *Am. Biotechnol. Lab.* **22**, 12–14 (2004).
65. Zhang, Y., Ge, C., Zhu, C. & Salaita, K. DNA-based digital tension probes reveal integrin forces during early cell adhesion. *Nat. Commun.* **5**, 5167 (2014).
66. Liu, Y., Galior, K., Ma, V. P.-Y. & Salaita, K. Molecular tension probes for imaging forces at the cell surface. *Acc. Chem. Res.* **50**, 2915–2924 (2017).
67. Gidi, Y., Bayram, S., Ablenas, C. J., Blum, A. S. & Cosa, G. Efficient one-step PEG-silane passivation of glass surfaces for single-molecule fluorescence studies. *ACS Appl. Mater. Interfaces* **10**, 39505–39511 (2018).
68. Woodside, M. T. et al. Nanomechanical measurements of the sequence-dependent folding landscapes of single nucleic acid hairpins. *Proc. Natl Acad. Sci. USA* **103**, 6190–6195 (2006).
69. Preibisch, S., Saalfeld, S., Schindelin, J. & Tomancak, P. Software for bead-based registration of selective plane illumination microscopy data. *Nat. Methods* **7**, 418–419 (2010).

Acknowledgements

We would like to thank S. Narum for carrying out FLIM and analysis, W. Weiss for sharing cell lines, W. Degrado and D. Sheppard for sharing integrin inhibitors and antibodies and O. Weiner and D. Sheppard for constructive comments. Funding for this work was provided by NIH NIGMS R35GM131766 to X.S. and NIH NIGMS R01GM131099 and R01GM124472 to K.S.

Author contributions

X.S. initiated the project. X.L. and X.S. designed the experiments and analyzed the data. X.L. conducted the experiments. D.C. and K.S. designed the tension experiments and analyzed the data. X.L., D.C., K.S. and X.S. wrote the paper.

Competing interests

The authors declare no competing interests.

Additional information

Extended data is available for this paper at https://doi.org/10.1038/s41589-023-01353-y.

Supplementary information The online version contains supplementary material available at https://doi.org/10.1038/s41589-023-01353-y.

Correspondence and requests for materials should be addressed to Xiaokun Shu.

Peer review information *Nature Chemical Biology* thanks Daniel Lietha, Adam W. Smith and the other, anonymous, reviewer(s) for their contribution to the peer review of this work.

https://doi.org/10.1038/s41589-023-01353-y

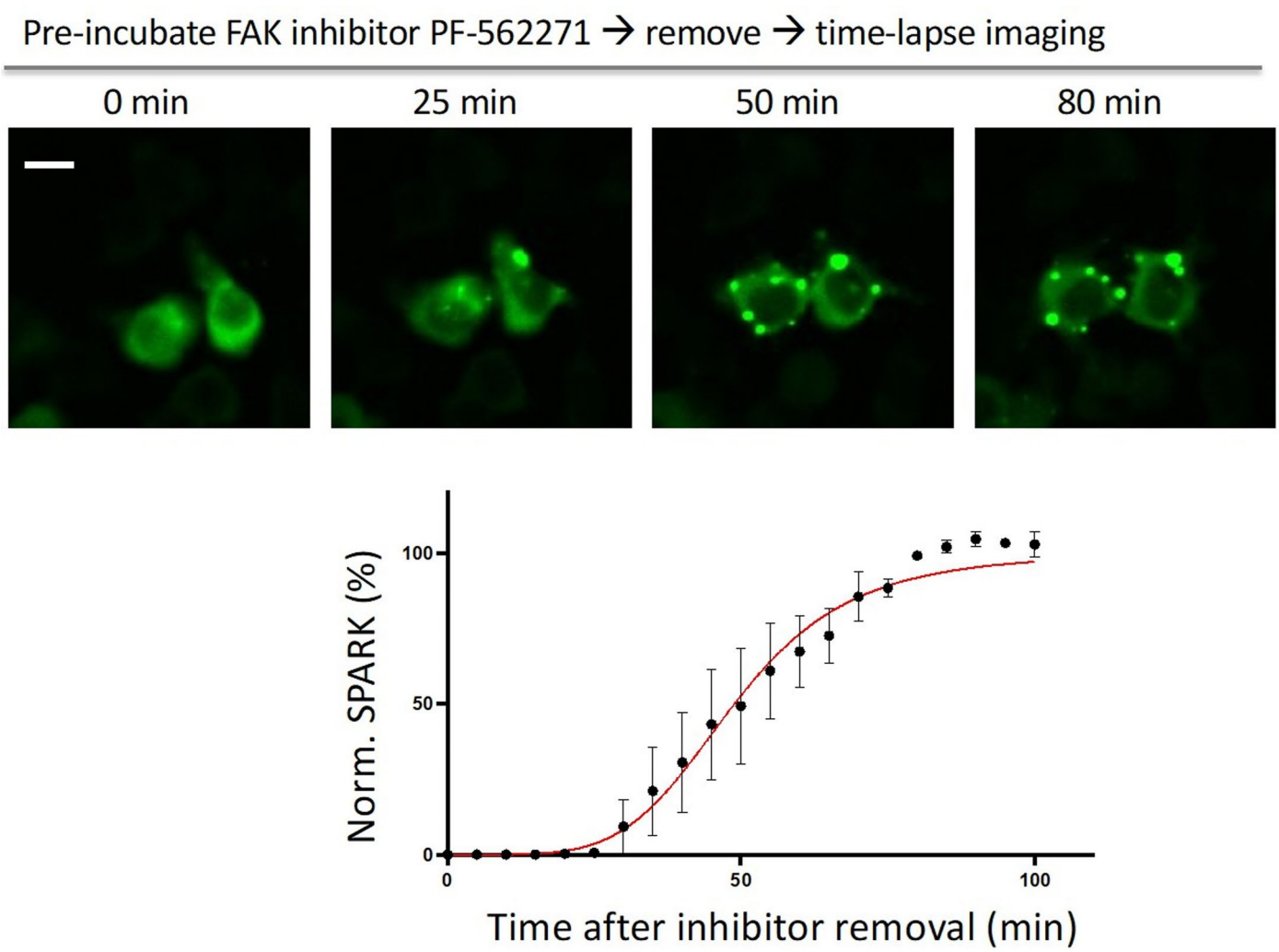

Extended Data Fig. 1 | FAK-SPARK forms droplets after removal of the FAK inhibitor. Data are mean ± SEM (n = 3 biological replicates). Scale bar, 10 µm.

https://doi.org/10.1038/s41589-023-01353-y

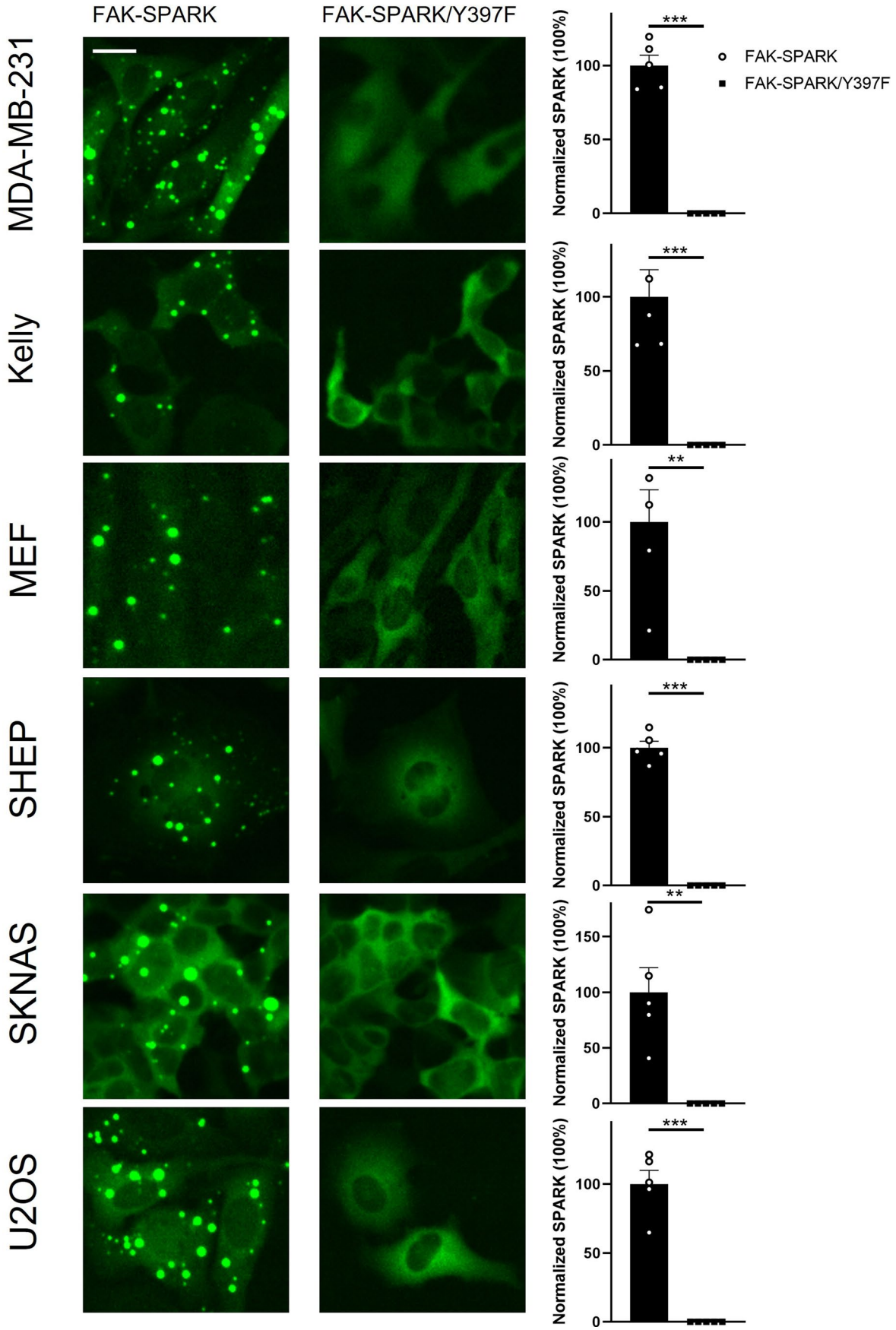

Extended Data Fig. 2 | FAK-SPARK is applicable to various cancer cells in imaging FAK activity using a lentivirus expressing FAK-SPARK. Data are mean ± SEM, n = 5 biological replicates, two-sided nonpaired t-test. $p = 5.52 \times 10^{-7}$ for MDA-MB-231, p = 0.00056 for Kelly, p = 0.0026 for MEF, $p = 2.64 \times 10^{-8}$ for SHEP, p = 0.0019 for SKNAS and $p = 8.17 \times 10^{-6}$ for U2OS). **: p value < 0.01. ***: p value < 0.001. Scale bar, 10 μm.

https://doi.org/10.1038/s41589-023-01353-y

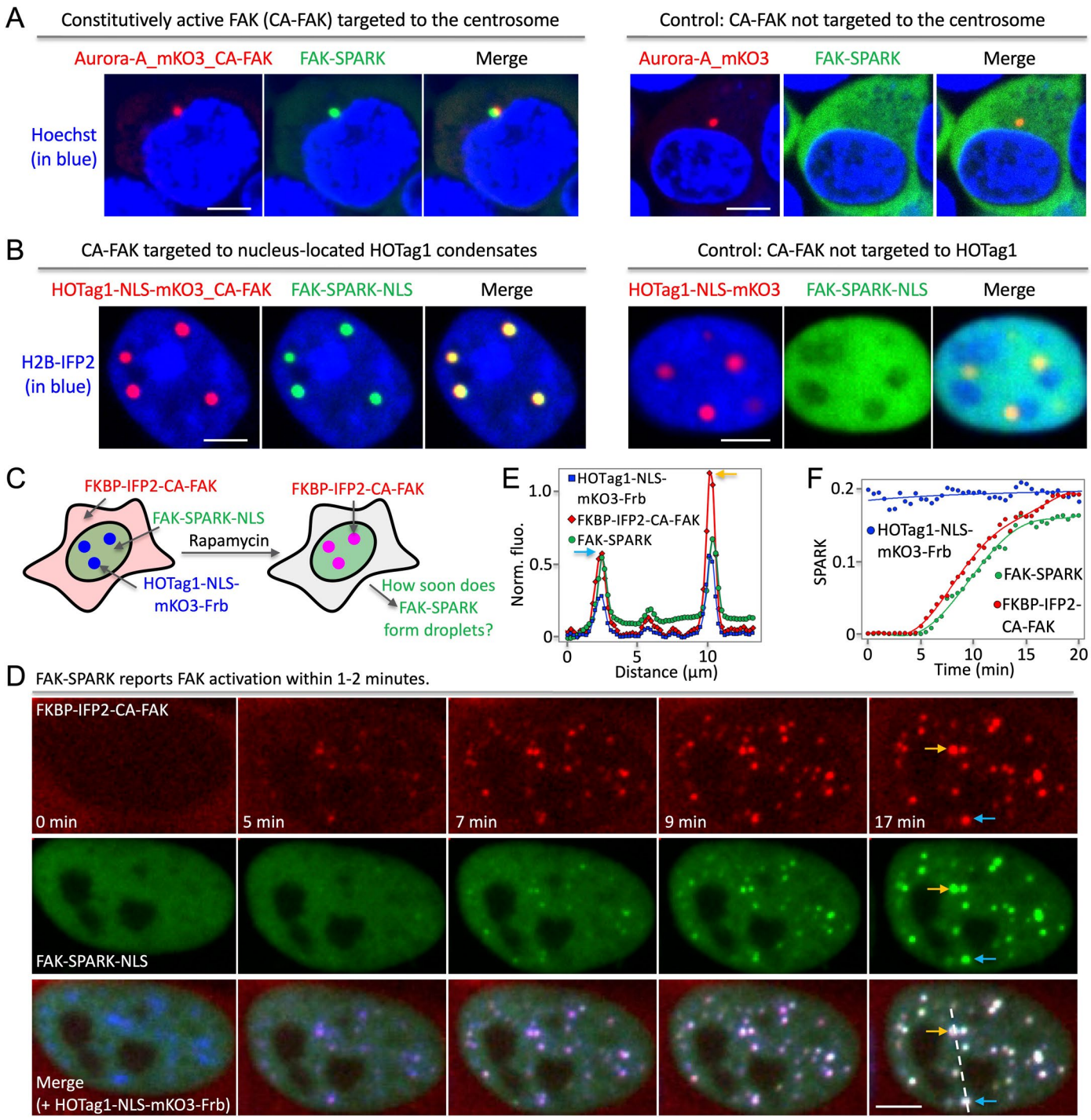

Extended Data Fig. 3 | FAK-SPARK visualizes FAK activity with spatiotemporal resolution by targeting active FAK into specific locations. **a** Fluorescence images showing that FAK-SPARK visualizes FAK activity in the centrosome when constitutively active FAK (CA-FAK) is fused to aurora A kinase that is located in the centrosome (left panels). FAK activity is absent in the centrosome without CA-FAK (right panels). **b** Fluorescence images showing that nucleus-located FAK-SPARK-NLS (nuclear localization signal) visualizes FAK activity in the nuclear HOTag1 condensates that are tagged with CA-FAK (left panels). FAK activity is absent the CA-FAK-absent HOTag1 condensates. **a** and **b** were repeated three times independently with similar results. (**c**) Cartoon showing experimental procedure of measuring FAK-SPARK temporal resolution. **d** Time-lapse images after addition of rapamycin. This experiment was repeated three times with similar results. **e** Normalized fluorescence along the dash line in (D). **f** Normalized SPARK signal over time. Scale bar, 5 μm (**a**, **b**, **d**).

https://doi.org/10.1038/s41589-023-01353-y

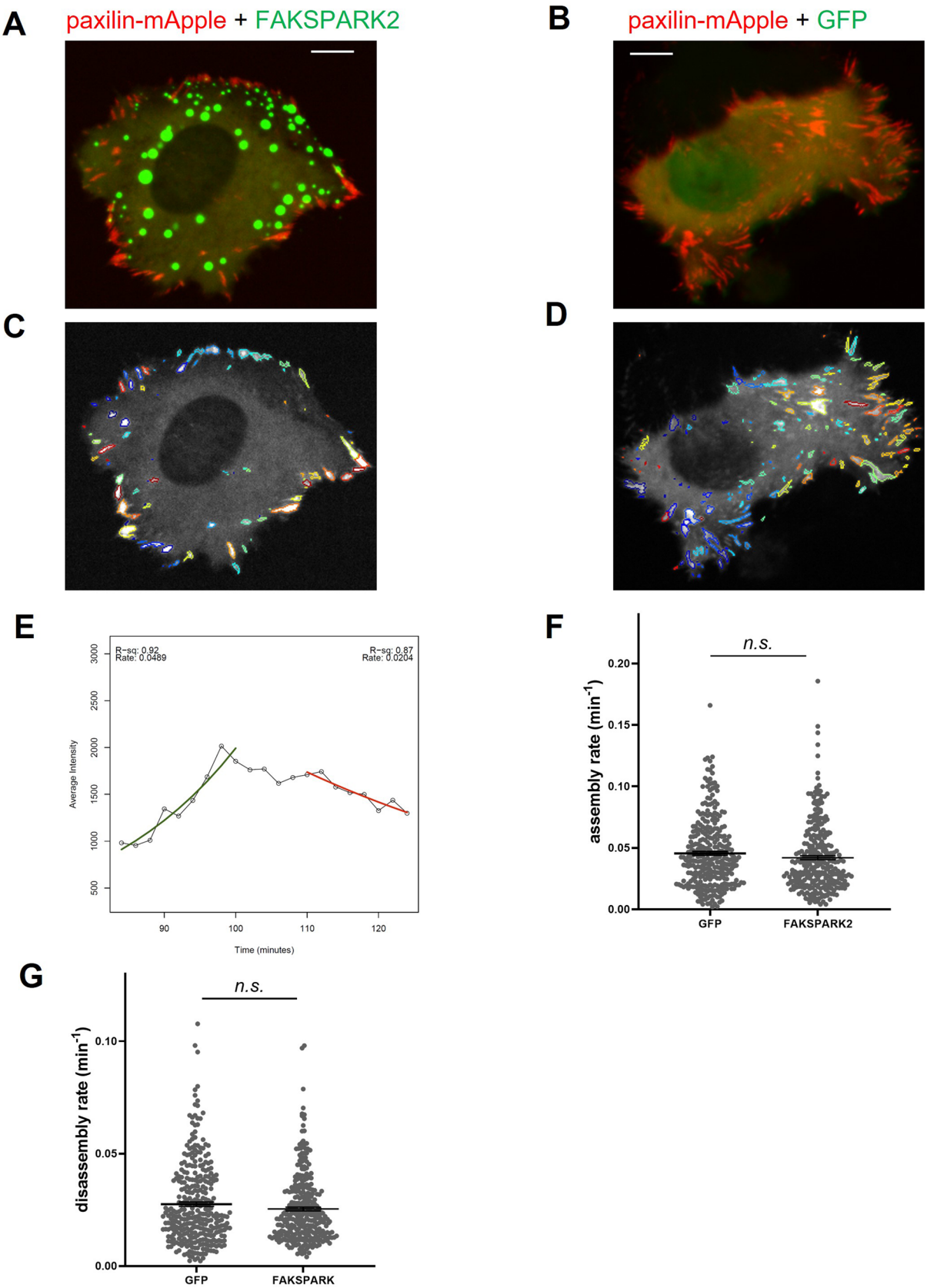

Extended Data Fig. 4 | FAK-SPARK expression does not perturb dynamics of focal adhesion assembly and disassembly. a, **b**, Representative images of HeLa cells expressing mApple-paxillin + FAK-SPARK and mApple-paxillin + GFP, respectively. **a** and **b** were repeated for three times independently with similar results. **c**, **d**, Tracking of FAs using Focal Adhesion Analysis Server {Steenkiste:2021iv, Berginski:2013dj} in **a** & **b**. **e**, A typical trace of assembly and disassembly rate calculation. **f**, **g**, Assembly rate and disassembly rate in HeLa cells expressing FAK-SPARK or GFP. two-sided nonpaired t-test, p = 0.12 and 0.10 for **f** and **g** respectively. Data represent mean ± SEM (n indicates FA numbers, 305 and 298 for GFP and FAK-SAPRK in **f**, 331 for both GFP and FAK-SPARK in **g**). Data represent mean ± SEM. *n.s.*, not significant. Scale=10 μm.

https://doi.org/10.1038/s41589-023-01353-y

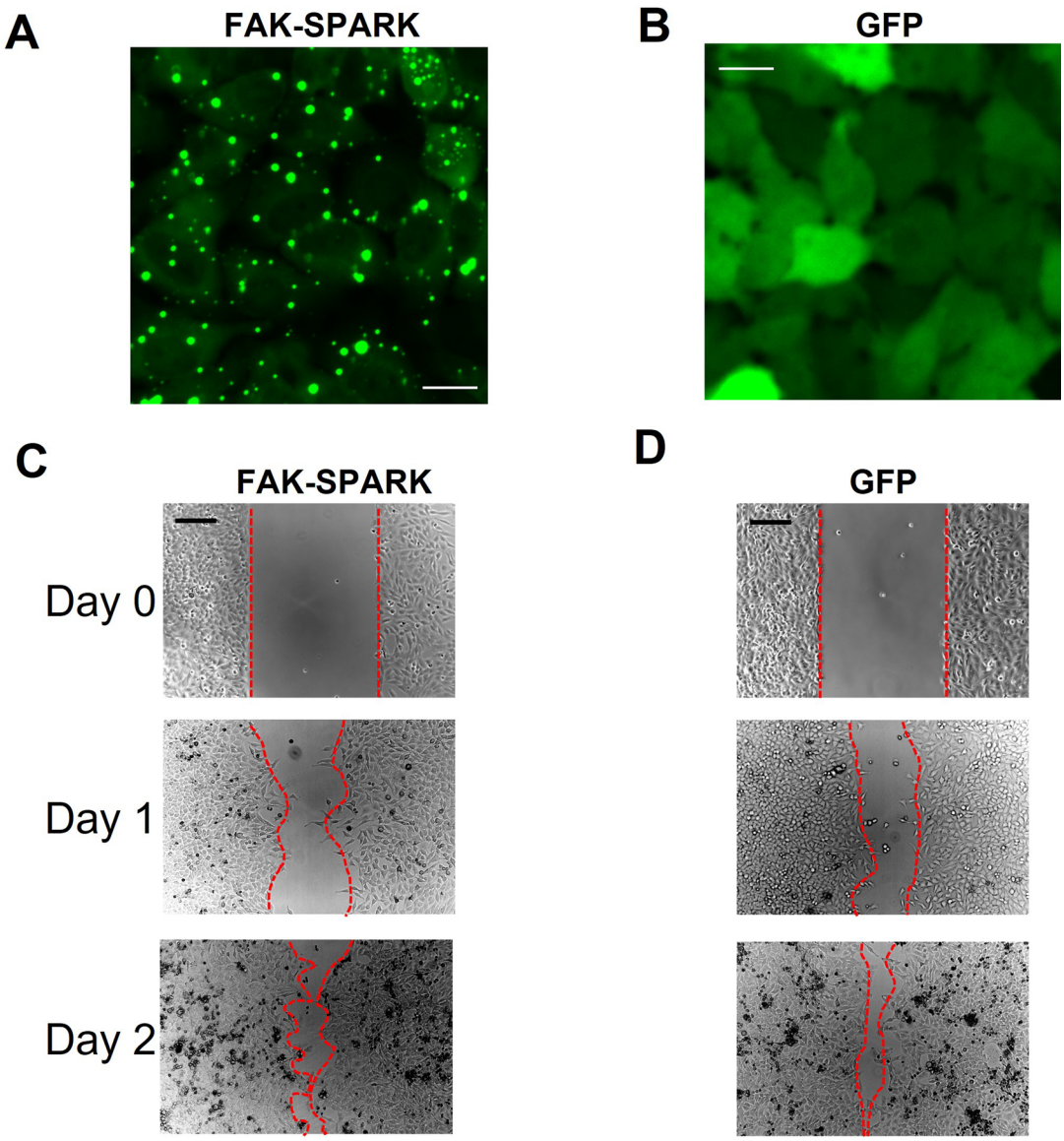

Extended Data Fig. 5 | See next page for caption.

https://doi.org/10.1038/s41589-023-01353-y

Extended Data Fig. 5 | FAK-SPARK expression does not perturb cell migration during wound healing using wound scratch assay. Wound was induced in HeLa cells expressing FAK-SPARK using a scratcher. **a**, **b**, Representative images of HeLa cells expressing FAK-SPARK or GFP, respectively. **c**, **d**, Typical images showing wound healing right after scratching (day 0), one day (day 1) and two days (day 2) after scratching. The red line marks cell boundary. **a**, **b**, **c** and **d** were repeated three times independently with similar results. **e**, Quantification of wound healing, n = 3 biological replicates. two-sided nonpaired t-test, p = 0.65 and 0.46 for Day 1 and Day 2. Data represent mean ± SEM. *n.s.*, not significant. Scale bar, 20 μm for A & B and 200 μm for **c** & **d**.

https://doi.org/10.1038/s41589-023-01353-y

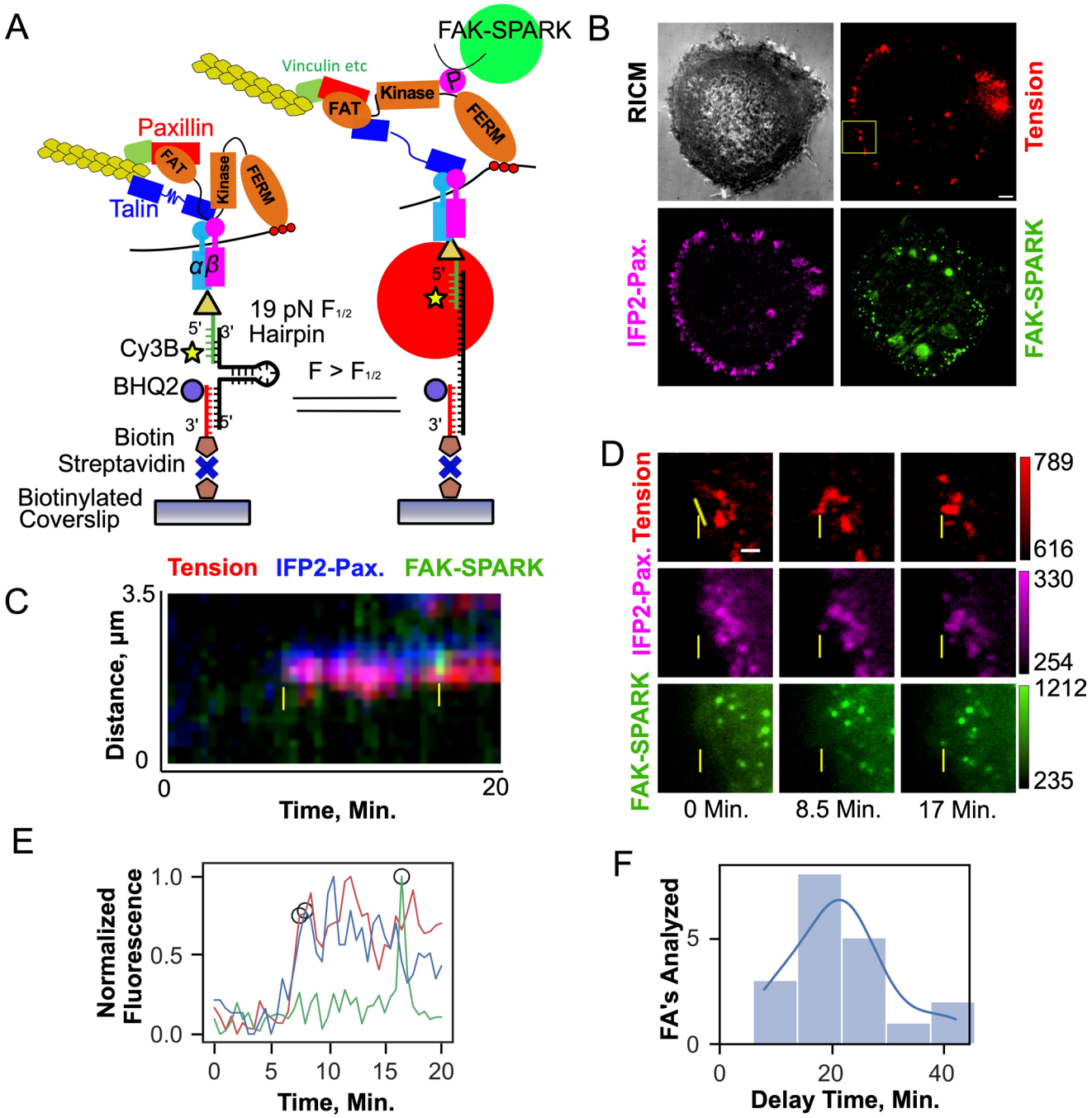

Extended Data Fig. 6 | Integrin-ECM ligand tension precedes FAK activity. **a** Diagram of 19 pN DNA-based MTFM probes and FAK-SPARK activation mechanism. **b** Representative cell RICM (gray) and fluorescence micrographs of 19 pN hairpin tension(red), IFP2-Paxillin(magenta), and FAK-SPARK(green) at t = 0.0 min. Scale bar, 5 µm. **c** Overlayed kymographs, yellow line in **d**, of tension, FAK-SPARK, and paxillin channels. Yellow arrows denote the point of tension and paxillin recruitment and FAK-SPARK droplet formation respectively. **d** Individual fluorescence micrographs of yellow inset in **b** at different timepoints, yellow dotted line denotes the linear ROI used for kymograph analysis in (c). Scale bar, 2 µm. **e** Plot of normalized maximum fluorescence over time derived from the kymograph, with threshold points used to derive the time delay denoted with black circles **f** Histogram of time delay measurements yielding 21.0 ± 9.0 min average delay between 19 pN integrin tension and FAK-SPARK droplet formation. n = 19 focal adhesions from 4 cells on 4 different surfaces (4 biological replicates).

nature portfolio

Corresponding author(s): Xiaokun Shu

Last updated by author(s): Apr 18, 2023

Reporting Summary

Nature Portfolio wishes to improve the reproducibility of the work that we publish. This form provides structure for consistency and transparency in reporting. For further information on Nature Portfolio policies, see our Editorial Policies and the Editorial Policy Checklist.

Statistics

For all statistical analyses, confirm that the following items are present in the figure legend, table legend, main text, or Methods section.

n/a	Confirmed
☐	☒ The exact sample size (*n*) for each experimental group/condition, given as a discrete number and unit of measurement
☐	☒ A statement on whether measurements were taken from distinct samples or whether the same sample was measured repeatedly
☐	☒ The statistical test(s) used AND whether they are one- or two-sided *Only common tests should be described solely by name; describe more complex techniques in the Methods section.*
☐	☒ A description of all covariates tested
☐	☒ A description of any assumptions or corrections, such as tests of normality and adjustment for multiple comparisons
☐	☒ A full description of the statistical parameters including central tendency (e.g. means) or other basic estimates (e.g. regression coefficient) AND variation (e.g. standard deviation) or associated estimates of uncertainty (e.g. confidence intervals)
☐	☒ For null hypothesis testing, the test statistic (e.g. *F*, *t*, *r*) with confidence intervals, effect sizes, degrees of freedom and *P* value noted *Give P values as exact values whenever suitable.*
☒	☐ For Bayesian analysis, information on the choice of priors and Markov chain Monte Carlo settings
☒	☐ For hierarchical and complex designs, identification of the appropriate level for tests and full reporting of outcomes
☒	☐ Estimates of effect sizes (e.g. Cohen's *d*, Pearson's *r*), indicating how they were calculated

Our web collection on statistics for biologists contains articles on many of the points above.

Software and code

Policy information about availability of computer code

Data collection	NIS-Elements AR v4.20 (Nikon) and Nikon Eclipse Ti were used to acquire images
Data analysis	ImageJ (1.53q), GraphPad Prism 8.0, Microsoft Excel (v2208) and the SymPhoTime Fast FLIM algorithm were used to process data.

For manuscripts utilizing custom algorithms or software that are central to the research but not yet described in published literature, software must be made available to editors and reviewers. We strongly encourage code deposition in a community repository (e.g. GitHub). See the Nature Portfolio guidelines for submitting code & software for further information.

Data

Policy information about availability of data

All manuscripts must include a data availability statement. This statement should provide the following information, where applicable:

- Accession codes, unique identifiers, or web links for publicly available datasets
- A description of any restrictions on data availability
- For clinical datasets or third party data, please ensure that the statement adheres to our policy

All data are available in the article, including the source data section.

Human research participants

Policy information about studies involving human research participants and Sex and Gender in Research.

Reporting on sex and gender	N/A
Population characteristics	N/A
Recruitment	N/A
Ethics oversight	N/A

Note that full information on the approval of the study protocol must also be provided in the manuscript.

Field-specific reporting

Please select the one below that is the best fit for your research. If you are not sure, read the appropriate sections before making your selection.

☒ Life sciences ☐ Behavioural & social sciences ☐ Ecological, evolutionary & environmental sciences

For a reference copy of the document with all sections, see nature.com/documents/nr-reporting-summary-flat.pdf

Life sciences study design

All studies must disclose on these points even when the disclosure is negative.

Sample size	No statistical methods were used to pre-determine sample sizes but our sample sizes are similar to those reported in previous publications (ref: Li 2021, doi: 10.1371/journal.ppat.1009898; Li 2023, doi: 10.1126/sciadv.ade3760)
Data exclusions	NO
Replication	All imaging experiments were repeated at least for 3 times with similar results.
Randomization	Different groups were all randomly grouped
Blinding	For experiment to determine the difference between FAK-SPARK and Y397F mutant, the difference in droplet signal is very distinct. For reseeding experiment, the GFP droplet revealing FAK activity in focal adhesion regions can be easily observed from imaging data.

Reporting for specific materials, systems and methods

We require information from authors about some types of materials, experimental systems and methods used in many studies. Here, indicate whether each material, system or method listed is relevant to your study. If you are not sure if a list item applies to your research, read the appropriate section before selecting a response.

Materials & experimental systems

n/a	Involved in the study
☐	☒ Antibodies
☐	☒ Eukaryotic cell lines
☒	☐ Palaeontology and archaeology
☐	☒ Animals and other organisms
☒	☐ Clinical data
☒	☐ Dual use research of concern

Methods

n/a	Involved in the study
☒	☐ ChIP-seq
☒	☐ Flow cytometry
☒	☐ MRI-based neuroimaging

Antibodies

Antibodies used	1. Anti-FAK(phospho Y397) antibody EP2160Y (abcam ab81298), 600X dilution. 2. Rabbit anti FAK antibody (Cell Signaling Technology,#3285), 600X dilution. 3. goat anti-rabbit IgG Alexa Fluor-488 (abcam ab15007), 1000X dilution 4. Anti-rabbit IgG (HRP-linked Antibody) Cell Signalling Technology, #7074S), 1000X dilution
Validation	1. Anti-FAK(phospho Y397) antibody EP2160Y, it was validated for IHC and WB against human cell in vendor website (https://

Validation	www.abcam.com/products/primary-antibodies/fak-phospho-y397-antibody-ep2160y-ab81298.html). Such application was also reported in previous paper (doi: 10.1080/21655979.2021.2024336). 2. Rabbit anti FAK antibody, it was validated for IHC and WB against human cell in vendor website (https://www.cellsignal.com/products/primary-antibodies/fak-antibody/3285). There is also paper using this antibody (doi: https://doi.org/10.1101/2021.10.23.465573). 3. goat anti-rabbit IgG Alexa Fluor-488, it was validated for IHC in vendor website (https://www.abcam.com/products/secondary-antibodies/goat-rabbit-igg-hl-alexa-fluor-488-ab150077.html). There is also paper using this antibody (doi: 10.1007/s11302-021-09829-z). 4. Anti-rabbit IgG (HRP-linked Antibody), it was validated for WB in vendor website (https://www.cellsignal.com/products/secondary-antibodies/anti-rabbit-igg-hrp-linked-antibody/7074?gclid=CjwKCAjw__ihBhADEiwAXEazJgScv9ZhmoArH2gyPqfJzToL4fnugBtHjuWh9BoZL6zbf1KY0N0_fhoC8pAQAvD_BwE&gclsrc=aw.ds). There is also paper using this antibody for WB (doi: 10.1126/sciadv.ade3760).

Eukaryotic cell lines

Policy information about cell lines and Sex and Gender in Research

Cell line source(s)	293T/17 (ATCC CRL-11268) Hela (Gift from Dengke Ma lab, UCSF) MDA-MB-231 (UCSF Cell Culture Core Facility) U2OS (Gift from Dengke Ma lab, UCSF) Kelly (Gift from William A. Weiss lab, UCSF) SHEP (Gift from William A. Weiss lab, UCSF) SKNAS (Gift from William A. Weiss lab, UCSF) 293FT cell (Gift from Young-wook Jun lab, UCSF) MEF (Gift from Dean Sheppard Lab, UCSF)
Authentication	None of the cell lines have been authenticated.
Mycoplasma contamination	Cell lines were not tested for mycoplasma contamination but no indication of contamination was observed.
Commonly misidentified lines (See ICLAC register)	No commonly misidentified cell lines were used.

Animals and other research organisms

Policy information about studies involving animals; ARRIVE guidelines recommended for reporting animal research, and Sex and Gender in Research

Laboratory animals	zebrafish in Ekkwill background , 2 day post fertilization
Wild animals	No wild animals were used in this study.
Reporting on sex	sex is not determined on 2 days post fertilization for zebrafish
Field-collected samples	No field-collected samples were used in this study.
Ethics oversight	The zebrafish work was performed as approved by the UCSF Institutional Animal Care and Use Program.

Note that full information on the approval of the study protocol must also be provided in the manuscript.